Investigation of inter-subject variation in ultrafine particle deposition across human nasal airways: A study involving children, adults, and the elderly

Science of the Total Environment 955 (2024) 177028

Contents lists available at ScienceDirect

Science of the Total Environment

journal homepage: www.elsevier.com/locate/scitotenv

Investigation of inter-subject variation in ultrafine particle deposition across human nasal airways: A study involving children, adults, and the elderly

Qinyuan Sun [a], Ya Zhang [b], Lin Tian [a,*], Jiyuan Tu [a], Richard Corley [c,d], Andrew P. Kuprat [d], Jingliang Dong [b,e,f,**]

[a] School of Engineering, RMIT University, Bundoora, VIC 3083, Australia
[b] Department of Otolaryngology Head and Neck Surgery, The Second Affiliated Hospital of Xi'an Jiaotong University, Xi'an, Shanxi 710004, China
[c] Greek Creek Toxicokinetics Consulting, LLC, Boise, ID 83714, USA
[d] Pacific Northwest National Laboratory, Richland, WA 99352, USA
[e] Institute for Sustainable Industries & Liveable Cities, Victoria University, Melbourne, VIC 8001, Australia
[f] First Year College, Victoria University, Footscray Park Campus, Footscray, VIC 3011, Australia

HIGHLIGHTS

- Impact of age-related anatomical changes on nasal particle deposition was studied.
- Deposition equations were developed using the combined diffusion parameter.
- Filtration efficiency in the main respiratory remains consistent across age groups.
- It paves the way for inhalation studies involving individuals across the life span.

GRAPHICAL ABSTRACT

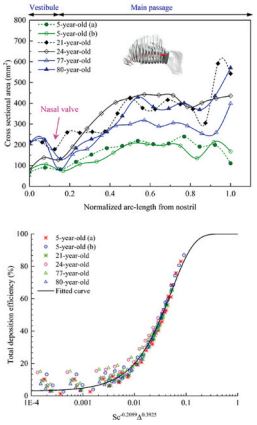

ARTICLE INFO

Editor: Meng Gao

Keywords:
Computational fluid particle dynamics
Nasal cavity
Age
Ultrafine particles

ABSTRACT

The airflow and particle dynamics in adult nasal airways have been extensively investigated, but the impact of age-related anatomical changes in children and the elderly remains underexplored. This study systematically investigates age-related anatomical variations and associated influence on nasal airflow dynamics and ultrafine particle deposition characteristics by using Computational Fluid-Particle Dynamics (CFPD) approach. Numerical simulations were conducted for 9 healthy nasal subjects spanning a wide age range. 6 Nasal subjects from the Development Group were used as the primary models for data analysis and deposition correlation development,

* Corresponding author.
** Corresponding author at: Institute for Sustainable Industries & Liveable Cities, Victoria University, Melbourne, VIC 8001, Australia.
E-mail addresses: lin.tian@rmit.edu.au (L. Tian), jingliang.dong@vu.edu.au (J. Dong).

https://doi.org/10.1016/j.scitotenv.2024.177028
Received 10 July 2024; Received in revised form 16 September 2024; Accepted 16 October 2024
Available online 20 October 2024

Deposition efficiency
Inter-subject variation

while 3 subjects from the Validation Group were used to validate the reliability of the derived total and sub-regional deposition correlations. Our results reveal distinctive variations across age groups. Specifically, the elderly and children exhibit unique patterns that differ from those of young adults. While total deposition efficiency differs significantly between children and adults, filtration efficiency in the subregion with most deposition, main respiratory, remains consistent. Lastly, overall and subregional empirical equations for deposition efficiency were developed by incorporating the combined diffusion parameter, $Sc^{a}\Delta^{b}$, corroborating the use of geometrical characteristic parameters for each specific subject in predicting nasal deposition efficiency across different age groups. Our findings are expected to improve the predictive nanoparticle exposure analysis in nasal airways across different age groups, thereby improving the respiratory health for individuals throughout the life span.

1. Introduction

With advancement of engineering and nanotechnology, nanoparticles have been incorporated into diverse environmental settings, from industrial workplaces to urban environments (Vaquero et al., 2016; Khezri et al., 2018). Extensive toxicological studies have demonstrated that exposure to nanoscale toxic aerosols can lead to a spectrum of health issues, encompassing sinusitis, nasal obstruction, alveolar inflammation, cardiovascular disease, and even mortality (Seaton et al., 1995). Given the growth in nanotechnologies and associated potential for airborne exposures to potentially toxic nanoparticulates, the intricacies of their deposition within the human respiratory system have garnered significant attention (Rahman et al., 2021; Seaton et al., 2010). To address the concern, a comprehensive exploration of nanoparticle deposition within the human nasal airway is imperative, as it serves as the primary line of defence in the human respiratory pathway, filtering airborne particulates (Noback et al., 2011; Elad et al., 2008). Inhaled airborne particles that are captured within the nasal airways are subsequently directed toward the mouth and oesophagus through the mucociliary clearance mechanism, which plays a pivotal role in reducing the risk of pulmonary exposure to toxic environments (Munkholm and Mortensen, 2014). The pronounced reliance of airborne particle exposure on this clearance mechanism and the anatomical structure emphasizes the pressing need for an in-depth investigation into nasal anatomy and its affected airflow behaviours.

While there have been extensive studies delving into the deposition of airborne nanoparticles within the human nasal cavity, a conspicuous gap exists in understanding variations in deposition patterns among distinct age groups. As numerous studies have clarified, age contributes to continuous morphological and physiological modifications in both the interior and exterior structures of nasal passages, which may alter the nasal airflow dynamics and associated filtration performance. During childhood and adolescence, growth and maturation can be the prime factor affecting nasal anatomy, such as in nasal height, philtrum length, and nasal tip protrusion-to-nasal height ratio, as frequently revealed in craniofacial measurements (Edelstein, 1996; Zankl et al., 2002; van der Heijden et al., 2008; Sforza et al., 2011). Besides external changes, statistically significant growth rates of intranasal space parameters in individuals under 17 years old was reported by Samoliński, et al. (Samoliński et al., 2007). Conversely, within the elder age group, studies in otolaryngology have commonly cited the phenomenon of a drooping nose tip, attributed to the loss of fibroelastic support (Parkes and Kamer, 1973; Cochran et al., 2007), which may shift the external environment as airflow enters the nasal pathway. Moreover, in addition to these changes over a lifetime, the physiological nasal environment also undergoes age-related shifts. Sakakura, et al. (Sakakura et al., 1983) reported that 31 % of 42 volunteer subjects aged over 60 years old did not achieve the expected mucociliary transport observed in younger subjects (aged under 60 years old) in their nasal mucociliary clearance measurements. Similarly, several studies have reported diminished mucociliary clearance performance in connection with the aging process (Kim et al., 2007; Proença de Oliveira-Maul et al., 2013). The age-related anatomical and physiological transformations may hold the key to differential nanoparticle exposure performance within the human nasal cavity, emphasizing the necessity of comprehending aerosol transport characteristics across age groups to enhance the tailoring of respiratory healthcare.

The investigation of fluid dynamics and ultrafine particle behaviour in the human nasal cavity has been the subjects of numerous *in vivo* and *in vitro* studies. Cheng, et al. (Cheng et al., 1996a) measured nasal airway dimensions and extra-thoracic deposition for ultrafine particles ranging from 4 to 150 nm in ten healthy adult volunteers. The results suggested a correlation between inter-subject variability in particle deposition and individual nasal dimensions, including total surface area, minimum cross-sectional area, and complexity. This emphasizes the significance of considering biological variability when developing population-wide dosimetry for inhaled ultrafine particles. *In vitro* experiments provided an alternative approach that allowed for more detailed and unlimited measurement of fluid and particle dynamics while avoiding the risk of hazardous aerosols exposure present in *in vivo* experiments. Cheng, et al. (Cheng et al., 1988) evaluated monodisperse NaCl aerosols ranging from 4.6 to 200 nm in an adult polyester nasal-larynx cast. They described the theoretical estimation of the nasal deposition efficiency based on the airflow rate and the diffusion parameter derived from the turbulent diffusion process in a straight pipe, indicating that turbulent diffusion dominated the mechanism for ultrafine particle deposition. In a subsequent *in vitro* study, this group expanded their number of replicas to four, including a 1.5-year-old child replica, in order to gain an initial assessment of age-related influences and to improve the estimation of deposition fraction in human nasal airway. This was achieved by reducing the dependence on the diffusion parameter in the equation (Swift et al., 1992). While most *in vitro* experiments focused on adult samples, this study extended the research scope to child subjects. Other researchers have also shifted their focus to morphological features of infant and child samples, as well as associated airflow and particle dynamics (Swift et al., 1992; Golshahi et al., 2010; Cheng et al., 1995a). By employing 10 infant replicas, Golshahi, et al. (Golshahi et al., 2010) reported significant deposition results for ultrafine particles ranging from 13 to 100 nm under both constant and tidal breathing conditions. They provided predictive correlations for infants, taking into account non-dimensional dynamical parameters, including Reynolds, Schmidt, and Womersley numbers, which incorporate geometrical features of nasal airways.

In addition to the *in vivo* and *in vitro* experiments, the growth in the development and application of computational fluid dynamics (CFD) modelling of human airways have contributed to our understanding of overall and local respiratory airflows and particle transport for a variety of ventilation and exposure conditions (Huang et al., 2001; Zamankhan et al., 2006; Wen et al., 2008; Inthavong et al., 2011; Moghadas et al., 2011; Garcia et al., 2015; Shang et al., 2022). Nevertheless, very few studies have considered the impact of anatomical variations due to growth in children and aging in the elderly on flow fields and particle motion. Xi, et al. (Xi et al., 2012) quantified the age-related impact on airway physiology, breathing resistance, and ultrafine aerosol filtering efficiency, both in total and in sub-regions, using a 10-day-old newborn, a 7-month-old infant, a 5-year-old child, and a 53-year-old adult. Despite significant differences in morphology and dimensions, no significant effects were observed on total deposition fractions or maximum local

deposition enhancement, while inter-subject differences were observed in the deposition in sub-regions of interest. Additionally, the child subjects pool was extended to unhealthy subjects due to the unique airway structure occurring in common diseases, providing more convincing evidence for importance of airway morphology in paediatric respiratory health care. Yang, et al. (Yang et al., 2024) investigated the impacts of severity levels of paediatric acute epiglottitis (AE) on aerosol transport characteristics. The angle of the epiglottis was artificially increased in a geometry from a healthy individual, mimicking severe AE. Their results indicated that the ideal particle size for drug treatment at the epiglottis region gradually decreased with larger angle of the epiglottis. Similarly, by comparing a severely obstructed nasal airway of a 3-year-old child with adenoid hypertrophy and that of a healthy child, Sun, et al. (Sun et al., 2023) reported that ideal particle size for increased site-dose at the adenoid area was 6–15 μm, the same in both healthy and diseased models. However, the healthy model showed higher regional dose than the diseased model.

Overall, these studies underscore the importance of accounting for significant biological variability across all age groups to gain a deeper understanding of nasal fluid dynamics and the associated risk of exposure to airborne particles in different age groups. In this study, we conduct a comprehensive analysis of age-related anatomical variations across three distinct age groups: children, young adults, and the elderly. We employed six nasal models: two 5-year-old children, a 21-year-old male, a 24-year-old female, a 77-year-old male, and an 80-year-old male, to offer a systematically comparison of airflow characteristics and a refined, age-specific particle filtration analysis, incorporating geometrical parameters into derived numerical models. This approach gives a method for predicting dosimetry in individuals for all age groups, both in terms of overall deposition and subregional deposition. Furthermore, three additional nasal models (a 5-year-old female, a 32-year-old female, and an 87-year-old male) were included for each age group to further justify and demonstrate the reliability of the developed total and subregional correlations. Our research not only provides invaluable insights into the complexities of deposition processes, but also paves the way for future studies aimed at population-wide dosimetry of airborne particles. This is especially important for informing risk assessment, particularly in vulnerable populations such as children and the elderly.

2. Method

2.1. Nasal airway models reconstruction

In this study, computed tomography (CT) images of nine human subjects across distinct age groups were adopted to reconstruct nasal cavity models. As shown in Fig. 1, the CT image data with a spatial resolution of 0.3 mm × 0.3 mm × 1.2 mm was employed to build the nasal models of adult individuals (a 21 years old Asian male, a 24 years old Asian female, a 77 years old Asian male, and an 80 years old

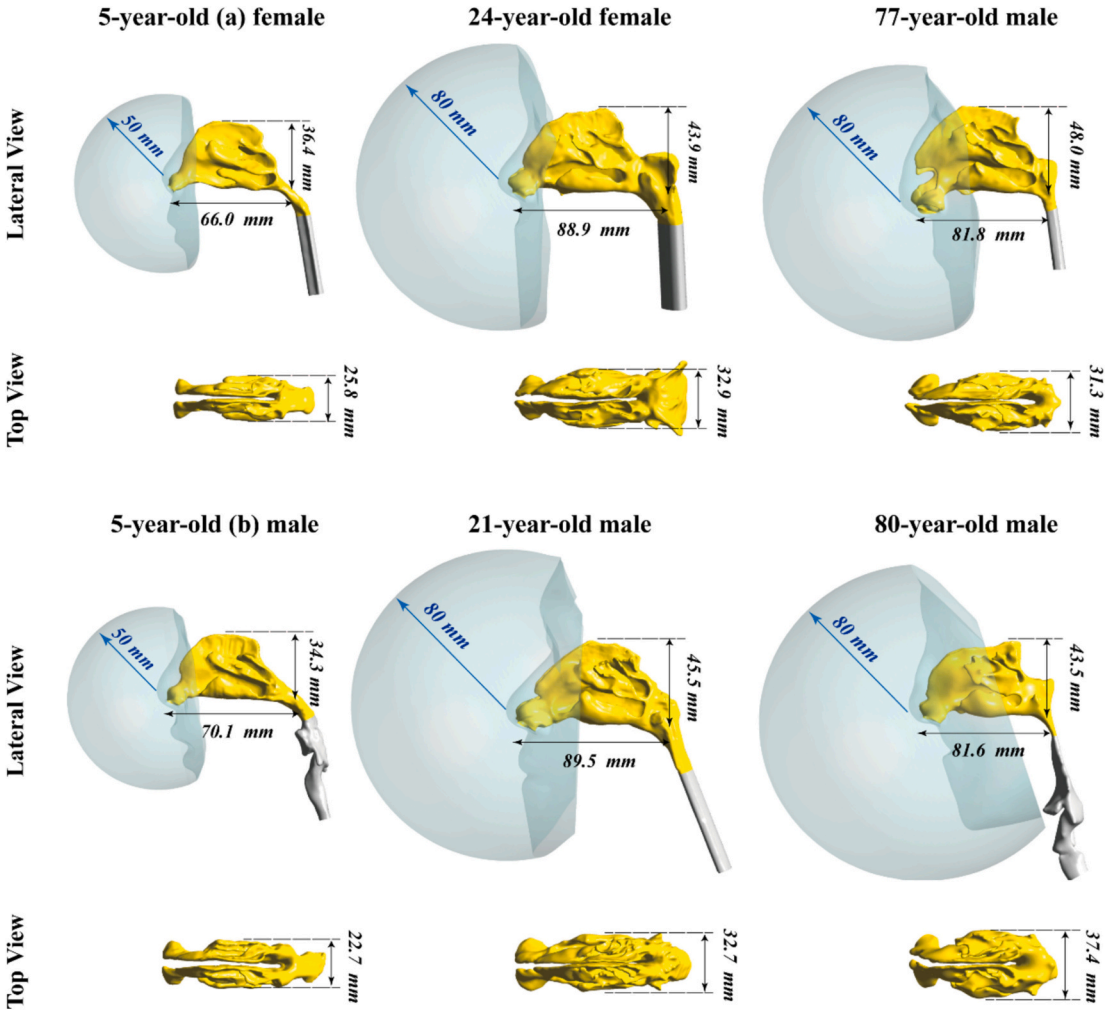

Fig. 1. Development Group nasal models for a 5-year-old female, a 5-year-old male, a 21-year-old male, a 24-year-old female, a 77-year-old male, and an 80-year-old male, with height and length marked in the lateral view and width marked in the top view. A spherical breathing zone is attached to the exterior facial features of each nasal geometry, with a diameter of 50 mm for child subjects and 80 mm for adult subjects.

Caucasian male). CT images with a spatial resolution of 0.3 mm × 0.3 mm × 0.5 mm were used to reconstruct the child models (a 5-year-old Asian female and a 5-year-old Asian male). These 6 nasal models were treated as the Development Group, where were used for flow and inhalation exposure data analysis and correlation development. In addition, three nasal models (a 5-year-old female, a 32-year-old female, and an 87-year-old male) were reconstructed from CT images as the Validation Group to assess the reliability of the developed overall and subregional deposition correlations. These additional nasal models are presented in Appendix Section, Fig. A3 and their demographic information is listed in Table A1 in Appendix. All models were based on existing medical data from the research team's previous projects, which were formally reviewed and approved by the human research committees at the Second Affiliated Hospital of Xi'an Jiaotong University and Pacific Northwest National Laboratory. All selected nasal airway subjects were healthy and had no diagnosed nasal conditions.

The sets of image data (DICOM format) were imported into 3D slicer version 5.0.3 (open-source platform [available http://www.slicer.org]) for nasal airway segmentation and smoothing. During rebuilding three-dimensional surface models, the external nose and surrounding facial details were retained and enclosed by spherical breathing zones. With addition of computational domain external to the face, more accurate fluid flow that transports particles could be simulated as discussed in previous studies (Shang et al., 2015a). A hemispheric breathing zone was established with an 80 mm radius for adult and elderly subjects, and a 50 mm radius for children. Meanwhile, an artificial extension was attached to the end of nasal pharyngeal region to obtain the fully developed airflow profiles in the pharynx with improved computational convergence. It should be mentioned that the larynx region of the 5-year-old (b) and the 80-year-old were preserved rather than using artificial extension (Fig. 1) and were not specifically considered in the aerosol deposition calculations as this falls outside of the current research scope and does not affect the analysis in this paper. The detailed model reconstruction process appears in our previous work (Inthavong et al., 2011; Inthavong et al., 2009; Dong et al., 2021a).

2.2. Mesh generation

Ansys Fluent Meshing (Ansys Inc., Canonsburg PA) was used to generate a polyhedral mesh for flow field solving. Compared with tetrahedral elements, a polyhedral mesh is more economical for computational resources since it generates far fewer cells and gives more accurate predictions at the same time (Wang et al., 2021). Fig. 2 is a preview of the internal mesh configuration of 5-year-old child model for example, with two typical cross-sectional views at nasal vestibule and main nasal passage. Maximum element sizes of 0.5 mm and 8.0 mm were used respectively for main nasal airway and external breathing zone, resulting in a polyhedral mesh containing 0.29 million polyhedral elements for the main nasal area and 0.05 million polyhedral elements for the external breathing zone. Mesh independence tests were conducted by generating three different mesh configurations: coarse mesh with 0.59 million grids, medium mesh with 1.03 million grids, and fine mesh with 1.3 million grids (Fig. A1 in Appendix Section). To balance computational cost and numerical prediction accuracy, medium mesh was employed in this study. This resulted in 8 prism layers of hexahedral elements being attached to the nasal wall and external nose area to better resolve the near-wall region flow behaviour with reducing skewness and non-orthogonality. This increased the size of the polyhedral-prism mesh for the main nasal area to 1.03 million elements. Based on the nasal anatomical and epithelial features, the nasal surface was divided into 4 subregions: nasal vestibule (dry squamous epithelium), main passage (mainly respiratory epithelium & transitional epithelium), olfactory (olfactory epithelium) and nasopharynx (Harkema et al., 2006; Schroeter et al., 2012; Shang et al., 2015b).

2.3. Boundary conditions and numerical modelling

Fig. 3 illustrates the measurement method of anatomical parameter, characteristic length, and the boundary conditions configuration. The characteristic length is the arc length measured from nostrils to the end of the nasopharynx (marked by the dashed red curve). It is used to

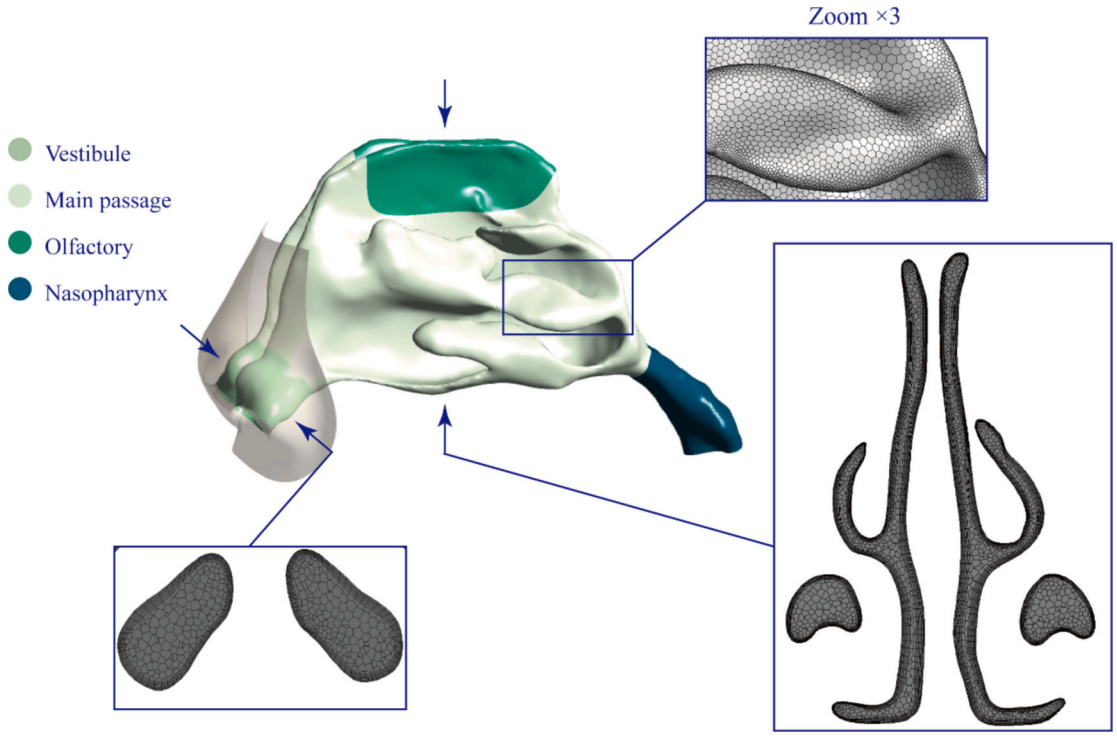

Fig. 2. Preview of a hybrid prism-polyhedral mesh: 5-year-old (a) female model was selected for example with internal mesh configurations at nasal vestibule, and main respiratory airway. Nasal airway was partitioned into vestibule, main passage, olfactory, and nasopharynx.

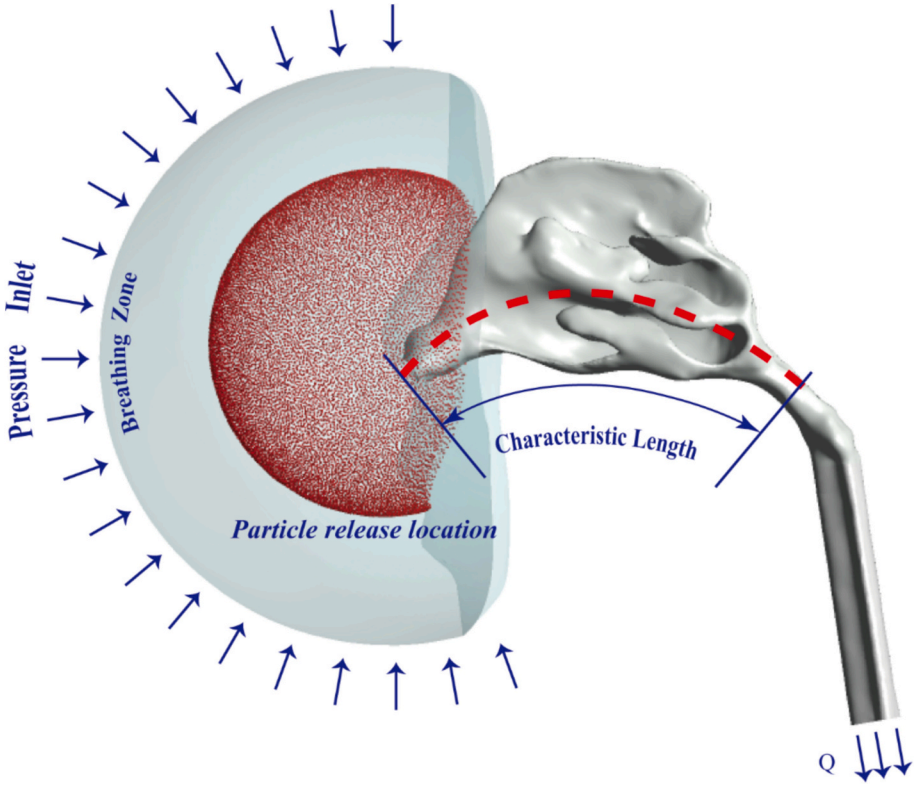

Fig. 3. Illustration of boundary conditions configuration and measurement of anatomical parameter: A spherical boundary serves as the inlet with atmospheric pressure, and the airway terminal serves as the velocity outlet. Airborne particles were uniformly released on the spherical surface with the centre at nose tip. The arc length from nostrils to the end of nasopharynx is the characteristic length (L), which used to calculate the combined diffusion parameter.

calculate the combined diffusion parameter (Section 3.5) and will be detailed discussed in later section. As shown in Fig. 3, the boundary of the breathing zone is defined as the inlet at atmospheric pressure to simulate the real inhalation environment. Exit flow rate is specified at the end of the artificial extension pipe at the nasal pharynx. Steady inhalation is assumed for all models and a wide range of inhalation flow rate is simulated for varied breathing conditions. According to ICRP (ICRP, 1994), the recommended parameters including tidal volume and respiration frequency for children and adults were listed in Table 1, based on which the inhalation flow rate under light exercise activity level were set as 9.5 LPM (Litre per minute) and 25 LPM respectively for children and adults in the current study.

Taking inter-subject variation into consideration, the individual outlet boundary flow velocity was determined by recommended volume rate divided by the outlet area of each model. Similarly, 3.1 LPM and 14.5 LPM are configured to represent the resting activity condition respectively for children and adults, with heavy exercise activity being assigned 9 LPM and 45 LPM for children and adults. All nasal surfaces were assigned the no-slip wall condition at room temperature.

The airflow was assumed as steady and incompressible, which was fundamentally governed by the incompressible Navier-Stokes equations. The continuity and momentum equations of the fluid flow are:

$$\nabla \bullet \vec{v} = 0 \tag{1}$$

$$(\nabla \bullet \vec{v})\vec{v} = -\frac{\nabla p}{\rho_{air}} + \frac{\mu}{\rho_{air}}\nabla^2 \vec{v} \tag{2}$$

where $\vec{v}$ represents the air velocity vector, p represents the static air pressure, and ρ_{air} is the density of air and μ is the air viscosity.

Though the specified flow rates provided moderate laminar flow in the main passage, the irregular intranasal structure contributes to complex flow regimes where the cross-sectional slice drastically changes, such as nasal valve or nasopharynx, or where the turbinate bones curl up to form convoluted pathways. In this study, the Shear-Stress Transport (SST) k-ω Model was employed for turbulence modelling. The SST form could effectively blend the accuracy of the k-ω model in the near-wall region and the robustness of the k-ε model in the outer part of the boundary layer (Yu and Thé, 2016; Rahman et al., 2019). It gradually transforms from the standard k-ω model in the inner region of the boundary layer to a high-Reynolds number version of the k-ε model in the far field (The standard k-ω model and the transformed k-ε model are blended by a function. The blending function is designed to be one in the near-wall region, which activates the standard k-ω model, and zero in the far field, which activates the transformed k-ε model.). More importantly, it accounts for the transport of the turbulence shear stress in the definition of the turbulent viscosity. Thus, it fits well with the characteristics for laminar-turbulent flow regimes in the nasal cavity.

As illustrated in Fig. 3, mono-dispersed particles with diameter of 1,

Table 1
Respiratory parameters under general light exercise activity level for children, adult and elderly subjects.

	5-year-old (a)	5-year-old (b)	21-year-old	24-year-old	77-year-old	80-year-old
V_T (L)	0.244	0.244	1.25	1.25	1.25	1.25
f_R (min^{-1})	39	39	20	20	20	20
A_{outlet} (m^2)	3.84e-05	7.17e-05	1.10e-04	3.19e-04	6.33e-05	1.27e-04
V_{outlet} (m/s)	4.12	2.21	3.78	1.31	6.58	3.29

1.2, 1.4, 1.6, 2, 3, 5, 7, 10, 30, 100 nm were passively released from a hemispherical surface with a radius of 30 mm centred at nose tip that fully overlays exterior nose. A particle number independence test was conducted using particle counts of 20,000, 50,000, and 100,000. The results indicated that the deposition efficiency curve for 50,000 particles closely overlaps with that for 100,000 particles (Fig. A2 in the Appendix). Consequently, 50,000 particles were released for each size at zero velocity and inhaled along airflow streamlines. Inertial impaction, gravitational sedimentation, and Brownian diffusion were considered as contributing mechanisms for particle deposition within the nasal cavity (Darquenne, 2020). Unlike the larger particles (> 0.5 μm) where inertial trajectories can deviate from airflow streamlines that change direction and impact on airway surfaces, Brownian diffusion, resulting from the random motions of the particles caused by their collisions with gas molecules, becomes the dominant mechanism of airway deposition for the ultrafine particles smaller than 200 nm (Cheng et al., 1988). Gravitational sedimentation is more efficient in the small airways and alveoli where lower flow rates, higher residence times and shorter travel distance contribute to particle deposition. For the predicted particles with size ranged between 1 and 100 nm, Brownian diffusion is considered as the dominant mechanism in the following discussion.

In this study, a one-way coupled Lagrangian discrete phase model (DPM) with low volume fraction was used to determine individual particle trajectories. The presence of swirls and eddies may contribute to a stronger mixing effect in turbulent flow, causing changes in both magnitude and direction of particle velocities and eventually causing nasal deposition. Taking the turbulent impact into consideration, the Discrete Random Walk (DRW) model was employed for particle simulation. Accounting for the drag force, gravity force, and Brownian force, the individual particle acceleration was determined by following force balance equation:

$$\frac{du_i^P}{dt} = f_D + f_G + f_B \tag{3}$$

where u_i^P represents the particles velocity with p referring to the particle phase, f_D is the drag force per unit particle mass defined by Stokes' drag law:

$$F_D = \frac{18\mu\left(u_i^g - u_i^p\right)}{C_c d_p^2 \rho_p} \tag{4}$$

here u_i^g represents gas flow velocity, μ is the air viscosity, d_P is the particle diameter, ρ_P is the particle density and C_c is the Cunningham correction factor calculated by:

$$C_c = 1 + \frac{2\lambda}{d_P}\left(1.257 + 0.4e^{\left(-\frac{1.1d_p}{2\lambda}\right)}\right) \tag{5}$$

Here λ is the air molecular mean free path (67 nm at body temperature of 310 K).

The Brownian force f_B, takes the form of a Gaussian white noise process defined as $\xi_i\sqrt{((\pi S_o)/\Delta t)}$, where Δt is the particle integration time-step and ξ_i is a zero-mean, unit-variance-independent Gaussian random number. S_o is a spectral intensity function:

$$S_o = \frac{216\nu k_B T}{\pi^2 \rho d_p^5 \left(\frac{\rho_p}{\rho}\right)^2 C_c} \tag{6}$$

where ν is the kinematic viscosity, k_B is the Boltzmann constant, T is the Kelvin temperature of inhaled air set as 310 K in this study. The current study employed Ansys Fluent 2020 R2 (Ansys Inc., Canonsburg PA) to perform numerical simulations.

Particles impacting the nasal surface were statistically counted as trapped and the particle deposition efficiency (*DE*) was calculated as follows:

$$DE = \frac{\#particles\ trapped\ by\ nasal\ wall}{\#particles\ entering\ nasal\ airway} \times 100\% \tag{7}$$

2.4. DPM model verification

To verify the reliability of present prediction models, rigorous validation was conducted by employing existing datasets collected from the literature. Fig. 4(A) depicted the datasets of deposition performance within paediatric subjects closely matched in age to our current child models. In addition to the resting condition (3.1 LPM), an additional inhalation flow rate of 7 LPM was simulated to facilitate comprehensive comparative analysis. First, a set of deposition data of a 5-year-old child was collected from a study by Xi, et al. (Xi et al., 2012), due to its remarkable congruence, both in age and nasal development process, with our current child models. At the flow rates of 3 LPM, our current results exhibited an impressive alignment with the reference data. Nevertheless, slightly wider gaps occurred for higher inhalation flow rate. This may be because of differences in data collection coverage, where Xi's study measured the region from nostrils to the laryngeal. In another study conducted by Cheng, et al. (Cheng et al., 1995a), upper airway deposition outcomes were ascertained by multiple clear polyester-resin casts generated from photographs. These cast featured paediatric individuals aged 1.5 years, 2.5 years and 4 years. Current results for high diffusion particles of 1 nm diameter highly agreed with the literature data, while the literature exhibited higher deposition efficiency for larger particle diameters. This may be attributed to the younger and smaller sized replica of a 4-year-old child that was used in the literature.

Fig. 4(B) presents validation for our adult subjects with 25 LPM inhalation flow rate. An *in-vitro* study by Cheng, et al. (Cheng et al., 1995b) assessed head deposition using replicas, which encompassing the nasal cavity, an oral passage, and a laryngeal-tracheal section, during both inspiratory and expiratory phases. Our current data exhibited excellent agreement under both 10 LPM and 20 LPM inhalation rates. Good agreement also was observed with a numerical study by Shi, et al. (Shi et al., 2008) that employing a 53-year-old model, as well as a study by Xi, et al. (Xi et al., 2012) that using a 53-year-old nasal laryngeal model. A minor gap was found between numerical data from Dong, et al. (Dong et al., 2018), who aiming to investigating the impact of vestibule phenotypes. Overall, current results achieve a high-level agreement with the literature data both in trend and magnitude, providing convincing evidence for the reliability of the following analysis and numerical models.

3. Results and discussion

3.1. Nasal airway morphological and dimensional analysis

Table 2 lists surface area in total and subregions, and the percentage in brackets defined as ratio of subregional area over total area. Overall, the child subjects showed smaller surface area and minor inter-subject discrepancy both in subregion and in total. For the surface area of vestibule, no significant difference was found in regional proportion. Notably, compared to children and young adults, the elderly exhibited the largest proportion (over 81 %) of airway in the main respiratory region, which may be attributed to the reduction of their nasopharynx surface area.

Table 3 lists intranasal volume and regional volume of enclosed vestibule, main passage (including olfactory region) and nasopharynx region. As expected, child subjects had much smaller volume than adult subjects both in total and in regions. Meanwhile, large inter-subject variability was observed between adult subjects. Literature data was presented for comparison purpose. Loftus, et al. (Loftus et al., 2016) reported that the average intranasal volume containing vestibule and main passage was 15.73 cm^3 (ranged between 11.13 and 24.25 cm^3)

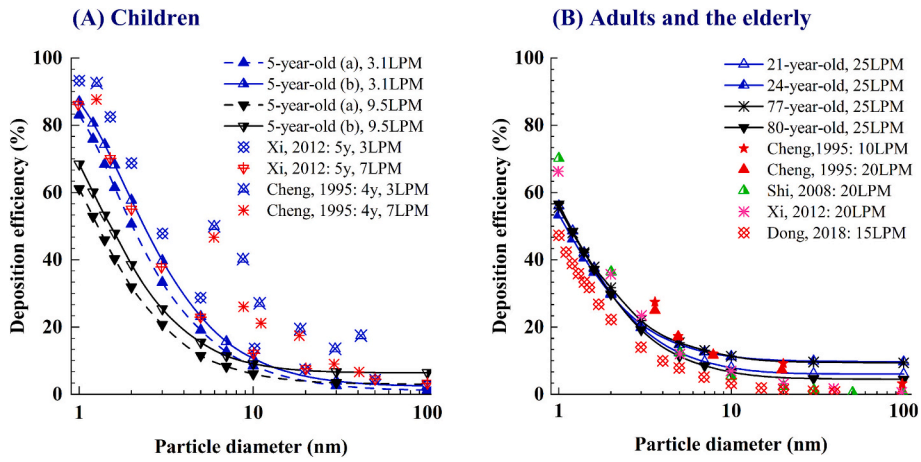

Fig. 4. Total deposition efficiency (%) and its comparison with existing literature data for (A) child subjects and (B) adult and elderly subjects.

Table 2
Detailed information of nasal surface area [cm^2].

	5-year-old (a)	5-year-old (b)	21-year-old	24-year-old	77-year-old	80-year-old
Vestibule	5.79 (4.8 %)	5.45 (4.7 %)	14.67 (6.4 %)	9.64 (4.8 %)	12.83 (6.2 %)	9.53 (4.6 %)
Main passage	96.34 (79.3 %)	90.08 (77.8 %)	176.23 (77 %)	142.75 (70.5 %)	166.81 (81.1 %)	169.81 (81.5 %)
Olfactory	12.38 (10.2 %)	13.36 (11.6 %)	15.93 (7 %)	14.86 (7.3 %)	14.62 (7.1 %)	15.77 (7.6 %)
Naso-pharynx	6.96 (5.7 %)	6.84 (5.9 %)	22.13 (9.7 %)	35.36 (17.5 %)	11.43 (5.6 %)	13.36 (6.4 %)
Total area	121.47	115.72	228.96	202.62	205.68	208.47

Table 3
Detailed information of nasal regional volume [cm^3].

	5-year-old (a)	5-year-old (b)	21-year-old	24-year-old	77-year-old	80-year-old
Vestibule	0.94 (7.2 %)	0.88 (7.1 %)	3.40 (9.4 %)	1.65 (4.0 %)	2.78 (11.6 %)	2.13 (7.1 %)
Main passage	10.60 (82 %)	9.91 (79.7 %)	25.39 (70.0 %)	24.58 (59.5 %)	17.48 (72.9 %)	23.51 (78.0 %)
Naso-pharynx	1.40 (10.8 %)	1.65 (13.3 %)	7.48 (20.6 %)	15.10 (36.5 %)	3.73 (15.6 %)	4.50 (14.9 %)
Total volume	12.94	12.45	36.27	41.33	23.99	30.14

among 22 subjects from age group of 20–30 years and 18.38 cm^3 (ranged between 13.64 and 25.04 cm^3) among 20 subjects from age group over 70 years. The measurement data showed consistency with elder subjects in this study, yet slightly smaller than that of young adult subjects in this study, especially the 21-year-old subject. Results of this study indicated slightly larger main passage volume in young adults than that of in elder adults. It should be noted that the elderly showed much smaller nasopharynx volume (3.73 cm^3 and 4.50 cm^3) than that of young adults (7.48 cm^3 and 15.10 cm^3), supporting the idea that a contracted nasopharynx likely to occurs in the elderly.

Fig. 5 quantifies the cross-sectional area (mm^2) aligning with the curvature of nasal geometry from nostrils to the start of nasopharynx. The first three data points were taken within vestibule, forming a curve that slightly increased and then decreased to a minimum at the nasal

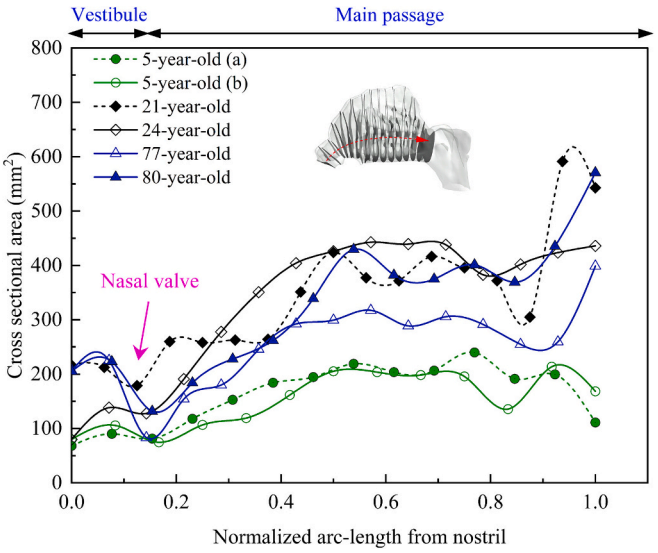

Fig. 5. Comparison of cross-sectional area along the nasal airway arc-length extending from the nostril to the nasopharynx.

valve that contributes around half of the airway resistance of total amount across the whole nasal cavity due to its narrow cross-section (Cole and Roithmann, 1996). With its narrow shape, the vestibule serves as the primary filtration portal for inhaled airborne particulates. In this region the child subjects exhibited a flatter cross-sectional area curve than in adult subjects. This indicates immature nasal vestibule shape with a more cylindrical-like and narrower pathway for inhaled airflow and particles among children. According to the reported data based on 25 adult subjects by Çakmak, et al. (Çakmak et al., 2003), bilateral nasal valve area ranged from 97 to 204 mm^2. Another measurement reported average unilateral minimal cross section area for different age group based on 165 participants, where 116 mm^2 for male and 90 mm^2 bilaterally for female under 50 years, and 128 mm^2 bilaterally for male over 80 years (Kalmovich et al., 2005). In this study, the average value was respectively 77.9 mm^2 for child models and 153.1 mm^2 for young adult models and 107.5 mm^2 for elderly adult models. Our results indicated a proportionately larger nasal valve area within young adult subjects in comparison to that of the elderly group (without considering mucosal engorgement). With nasal height elongating and the turbinate bone folding to develop into a lateral scroll-shape slit that connects the paranasal sinuses, cross sectional area in the main passage experienced a steady increase, where child subjects showed obviously a

narrower pathway than adult subjects. For adult subjects, no significant age impact is observed but the 77-year-old showed a much narrower airway than other adults. Interestingly, in the last two slices, where two chambers merged into the nasopharynx, the adult's curves showed an upward trend relative to the main airway, while the opposite occurred in the child group.

Internal structure through coronal slices was also analysed by hydraulic diameter defined as 4 times the ratio of cross-sectional area to perimeter of each coronal slice as shown in Fig. 6. This dimensionless parameter indicates an equivalent radius of cross-sectional nasal airway space, where smaller hydraulic diameter reveals narrower channels with higher rates of deposition of particles by diffusion. A distinguishing characteristic between children and adults could be observed in the vestibule region, where most adult subjects showed a consistent decrease from a peak value of around 10.7 mm, yet child subjects tended to be stable between 6.17 mm and 7.42 mm. As for the abnormal stable profile for the 24-year-old, it maintained a positive correlation with its smaller cross-sectional area of vestibule. In the main passage, the hydraulic diameter gradually decreases to a steady minimum level throughout turbinate region, following by a rapid increase in the posterior section especially in adult subjects. It is worth noting that young adult subjects showed slightly larger hydraulic diameter above 4.2 mm than that of children and elder subjects, indicating a wider diffusion equivalent diameter for particles.

In Fig. 7, complexity, is defined by the ratio of the square of the perimeter to the area of coronal slices throughout the nasal airway, with higher values suggesting more irregular and complex shapes. The complexity kept a very low value in the vestibule. Then in posterior region, it climbed to a peak value in the middle of main passage. The significant increase suggested more complex structure produced by the turbinate bone that curled toward the airway. It is noted that highest magnitude was achieved by the elderly group, which reflected much higher pathway complexity than that of children and young adult subjects. The normalized arc distance of reaching maximum value for the elderly was at 0.5–0.6, which is shorter than 0.7–0.8 in the children and young adult group.

3.2. Comparative analysis of airflow characteristics

Fig. 8 presents a comparative insight of airflow streamlines at the light exercise activity level. The velocities were normalized for clarity,

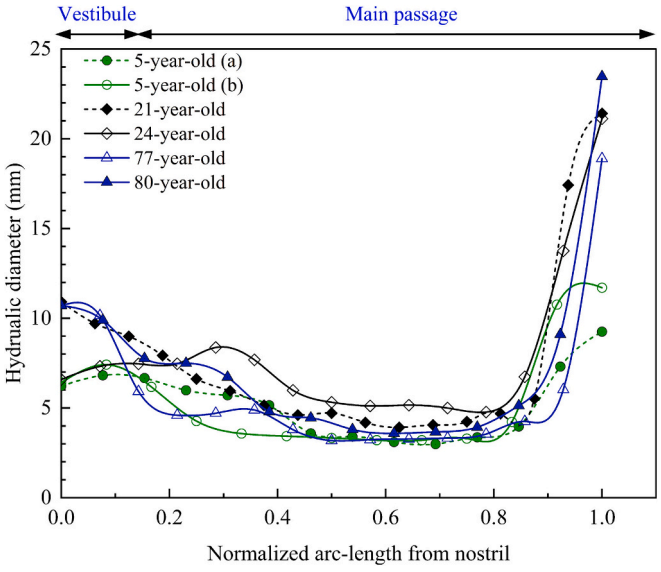

Fig. 6. Comparison of hydraulic diameter along the arc-length of nasal airway from the nostril to the nasopharynx.

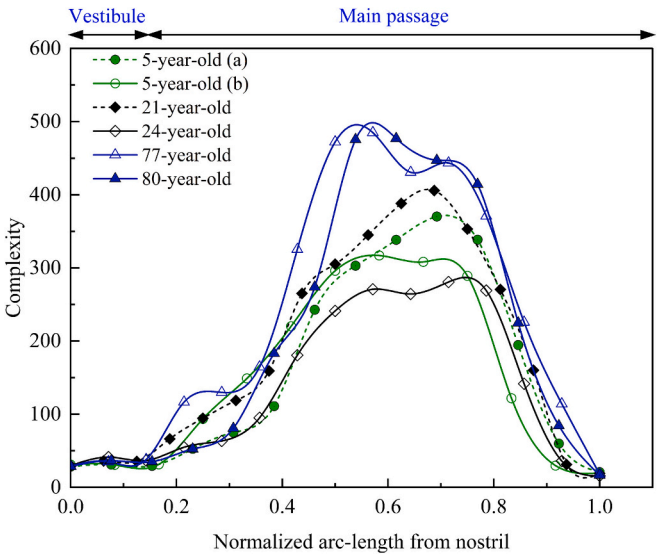

Fig. 7. Comparison of complexity along the arc-length of nasal airway from the nostril to the nasopharynx.

as the inhalation flow rates varied across different age groups. In general, main flow undergoes significant directional changes within nasal airway, forming a nearly 90-degree bend from nostrils to the nasopharynx. High-velocity regions are typically observed in the anterior and posterior of airways, where the nasal airway constricts abruptly. In the child models, much of the turbinate surface was in direct contact with the prevalent flow currents. High-velocity streams occurred near the vestibule in both child models, with peak velocities of 3.4 m/s and 3.6 m/s, respectively. Notably, child models exhibited a more organized, unidirectional downstream in the nasopharynx region, with no recirculation, distinguishing them from adult subjects. In the young adult models, the airflow was predominantly directed through the widest meatus of the nasal cavity – the middle meatus. Compared with the 21-year-old model, the 24-year-old model presented high-speed flows near the vestibule, with a peak velocity of 7.3 m/s. In contrast to the airflow patterns observed in children and young adults, peak airflow velocity in the elderly was detected in the extremely constricted nasopharynx region, with a peak velocity at 16.1 m/s. Furthermore, significant inter-subject variations were observed between the elderly. A unique notch at the top of the vestibule region occurs in the 77-year-old model, which restricted the downstream airflow direction and contributed to a pronounced recirculation zone at the anterior portion of the main passage. It may prolong the residence time for particles in that region and increase the possibility for particles to be captured by the nasal surface.

Fig. 9 illustrates the comparison of Wall Shear Stress (WSS) distribution on the bilateral nasal surfaces for all six considered models under the light exercise activity level. As expected, the patterns of WSS distribution closely align with the velocity profiles of the adjacent airflow fields. Evaluated WSS occurred in the regions characterized by increased near-wall velocity gradients.

Specifically, areas of high WSS trend to manifest in the nasal vestibule and nasopharynx due to abrupt airway obstructions. For the 5-year-old models (a) and (b), high WSS was observed in nasal vestibule, spreading across the inferior turbinate, and peaking in nasopharynx at 0.56 Pa and 0.78 Pa, respectively. Conversely, notable inter-subject variations of WSS distribution were discerned among the adult models. The inferior turbinate region experienced relatively high WSS, extending into the nasopharynx with a peak value of 0.85 Pa for the 21-year-old subject. In the contrast, the 24-year-old subject exhibited increased WSS primarily in the anterior airway, including the vestibule and anterior middle turbinate, especially in the right chamber, with a relatively higher value of 1.60 Pa. For the elder-adult subjects,

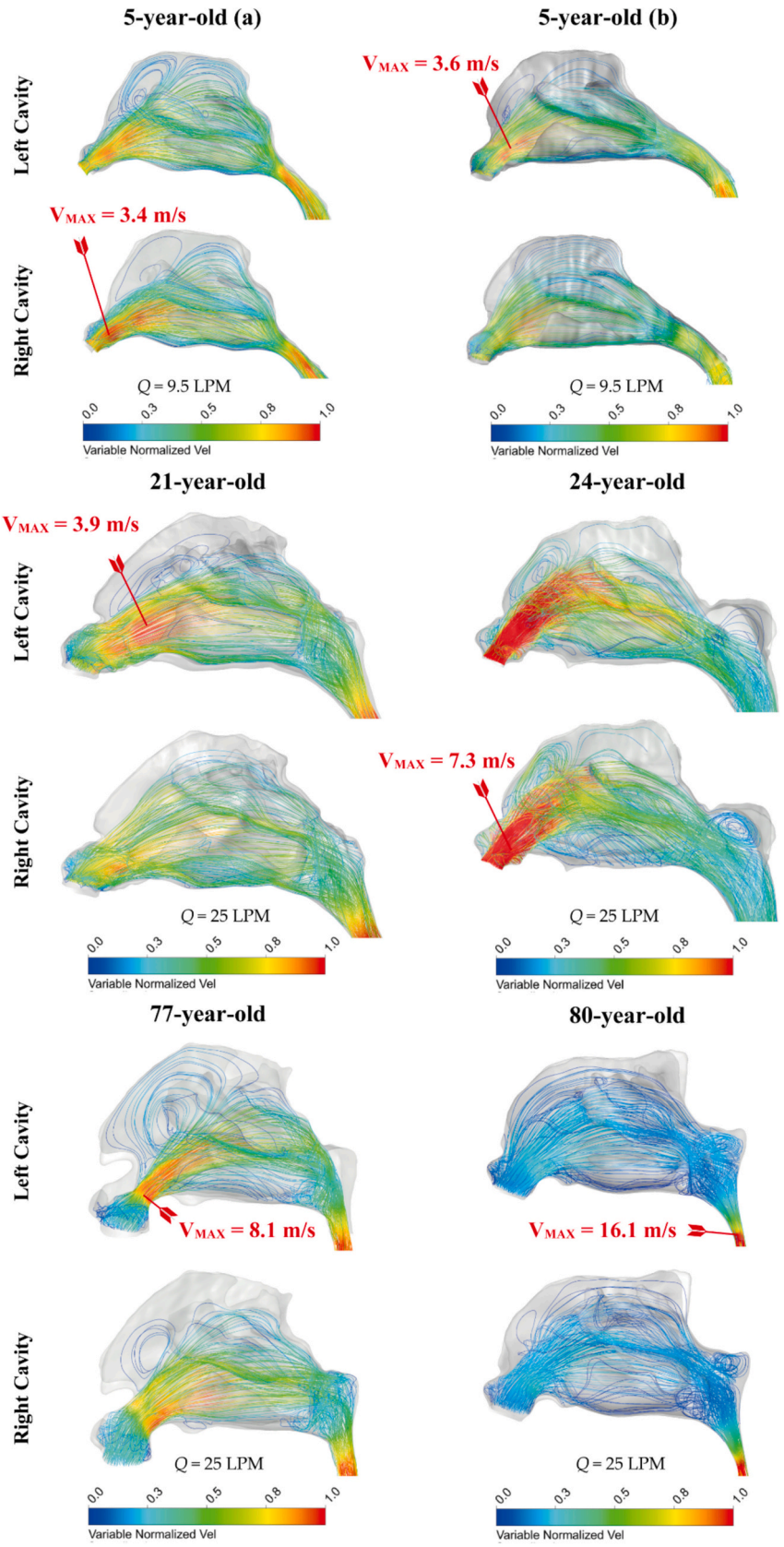

Fig. 8. Comparison of airflow streamlines with normalized velocity under light exercise activity level (9.5 LPM for children and 25 LPM for adults) in left and right cavities.

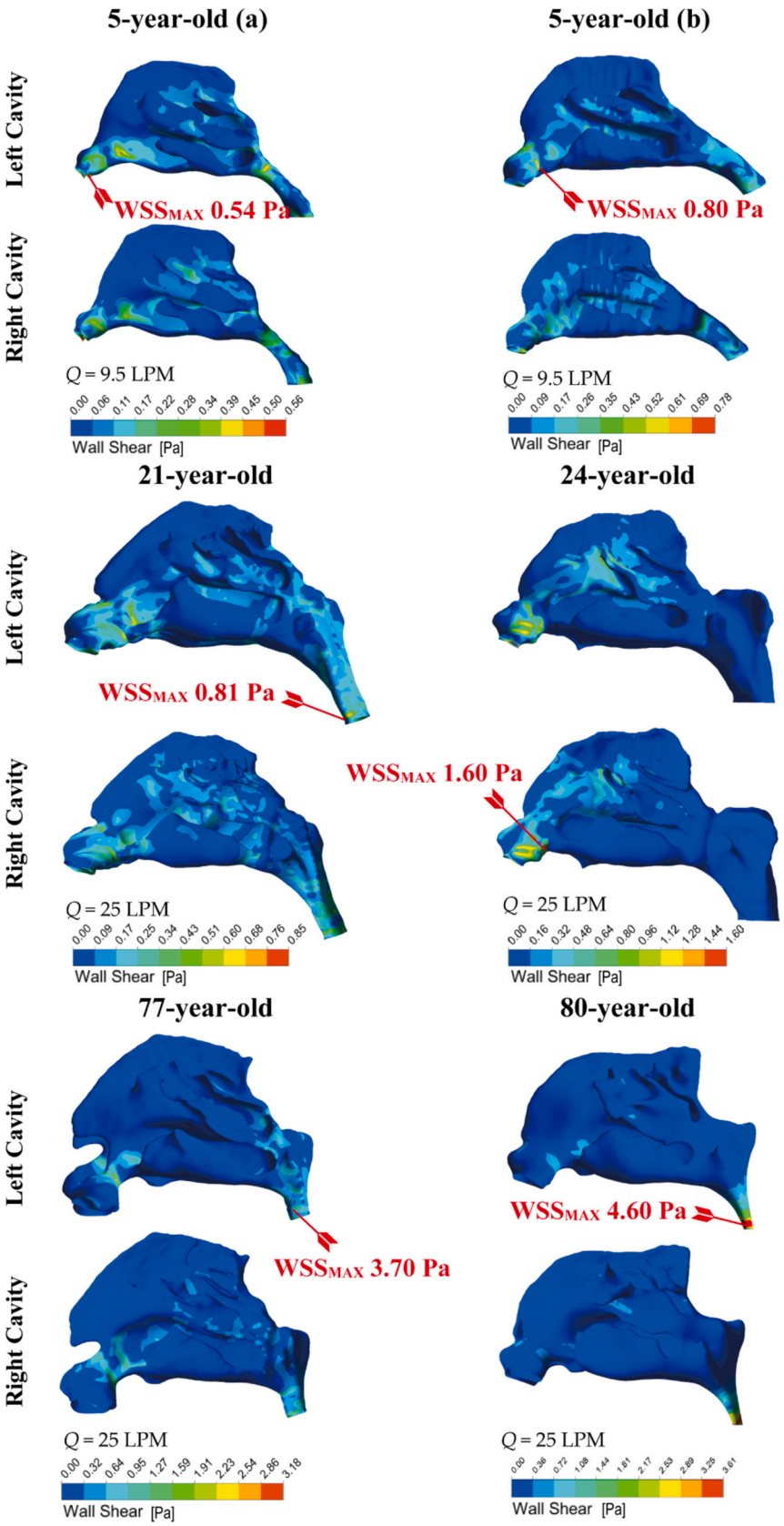

Fig. 9. Distribution of wall shear stress in the left and right nasal cavities under light exercise inhalation condition (9.5 LPM for children and 25 LPM for adults).

dramatically elevated WSS was observed near nasopharynx, owing to the severe airway constriction. The maximum magnitudes reached 3.18 Pa for the 77-year-old and 3.61 Pa for the 80-year-old. It is noteworthy that the observed high WSS values in elder subjects were roughly four times higher than those of the child subjects and triple those of the young adult subjects.

3.3. Spatial distribution of deposited particles

Fig. 10 illustrates the comprehensive spatial deposition visualization for nanoparticles with diameters of 1 nm and 10 nm under light exercise breathing conditions. In general, there was a pronounced tendency for extensive dispersion throughout the nasal cavities in all considered models. Relatively dense deposition occurred in the vicinity of primary airflow, particularly conspicuous on the vestibule and main passage.

Significantly, while noticeable inter-subject disparities of deposition patterns were found among adult subjects, similar deposition tendencies were evident in child subjects. Specifically, highly diffusive particles tended to deposit spread across all subregions of the slender nasal airways in children, particularly accumulated within the vestibule and middle turbinate. In the 21-year-old model, substantial amounts of particles were filtered by the vestibular region and subsequently transferred into the middle turbinate region, extending into the nasopharynx. However, in the 24-year-old, areas of heightened deposition were primarily concentrated within the anterior regions of the main passage, with minimal capture occurring within the nasopharynx.

For the elderly, particles exhibited concentrated deposition within the vestibular region like the younger adult subjects. However, in the elder subjects, deposition primarily concentrated on the upper wall of the nasal vestibule which can be attributed to the sharper turns undergone by the entering airflow. Notably, higher deposition was observed in the middle turbinate region where high-speed inhaled flow jets occurred in the 77-year-old model, while wide-spread patterns occurred across middle and upper turbinate regions for the 80-year-old model. Since inertial deposition is minimal for 1 nm or 10 nm particles, higher deposition is not due to the high-speed flow but is due to the low hydraulic diameter (which occurs where flow speed is high).

As anticipated, substantially reduced deposition patterns were observed when the particle diameter was increased tenfold to 10 nm, whereas the preferred deposition area for each individual model did not undergo obvious changes compared to the deposition patterns observed with 1 nm particles.

3.4. Overall and regional deposition efficiency

Respiratory activities vary dynamically in daily life. In Fig. 11, we show results of deposition efficiency under three activity levels as a function of particle diameter, encompassing resting, light exercise, and heavy exercise. In general, the function curves displayed a consistent trend, which declined with larger particle diameter and higher inhalation flow rates. This phenomenon can be attributed to the optimal interplay of Brownian force, which is maximized at lower flowrates where residence time is greater than that provided by more moderate convection flow.

Fig. 11(A) illustrates the results for the child group. The peak deposition value was unsurprisingly observed at 1 nm under the lowest inhalation flow rate (resting) and ranged between 83 % - 87 %. Notably, when transitioning from resting to light or heavy exercise conditions, a significant reduction was observed in the functional curves, which was not as great among adults. It should be specifically noted that as particle diameter increases, all deposition curves cross over and become higher for faster flow than for slower flow (as emphasized in the partial enlargement diagram). This reflects the trade-off between the enhanced inertial impaction promoted by higher flow rates and the diminished Brownian motion due to increasing particle diameter. At higher flow rates, the increased inertial impaction resulting from larger particle diameters suppresses the decline in deposition curves caused by reduced Brownian motion. Therefore, the curves tend to be plateau at the higher flow rate, rather than show a downward trend at the lower flow rate.

Fig. 11(B) represents the four adult subjects: the 21-year-old, the 24-year-old, the 77-year-old, and the 80-year-old models. Remarkably, with increasing inspiratory flow rates, a significant trend became evident: the gap between the peak deposition values of each individual progressively narrows, which was not found in paediatric models. Specifically, the deposition efficiency curves for the 21-year-old and the 80-year-old models displayed remarkable similarity across all particle sizes and

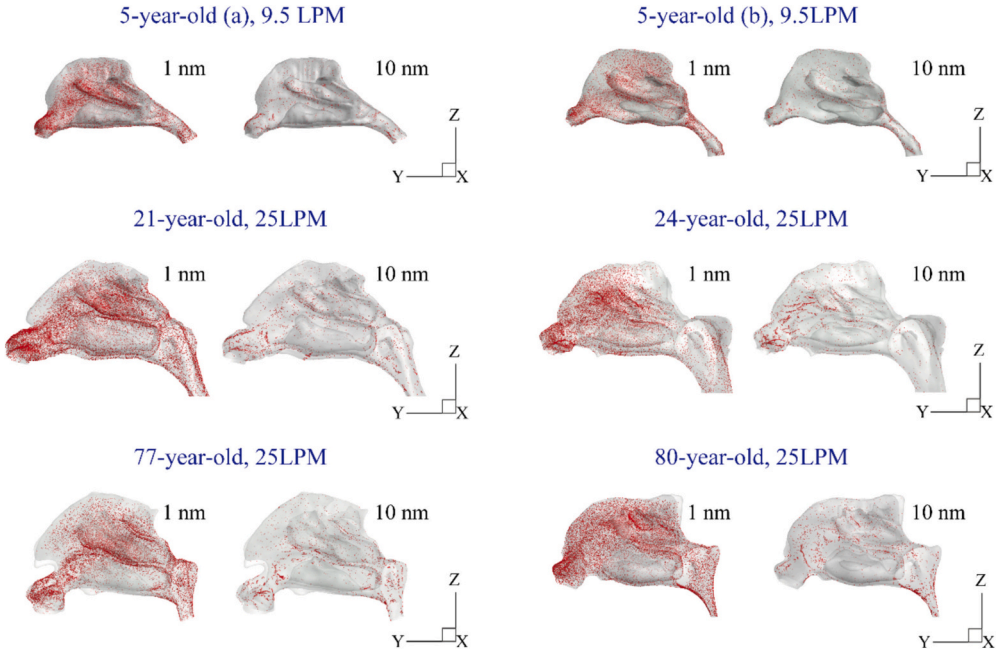

Fig. 10. Spatial nanoparticles deposition locations under light exercise inhalation conditions (9.5 LPM for children and 25 LPM for adult elderly subjects). Particle diameter of 1 nm and 10 nm were selected to preview deposition patterns respectively for higher-diffusion and weaker-diffusion situations.

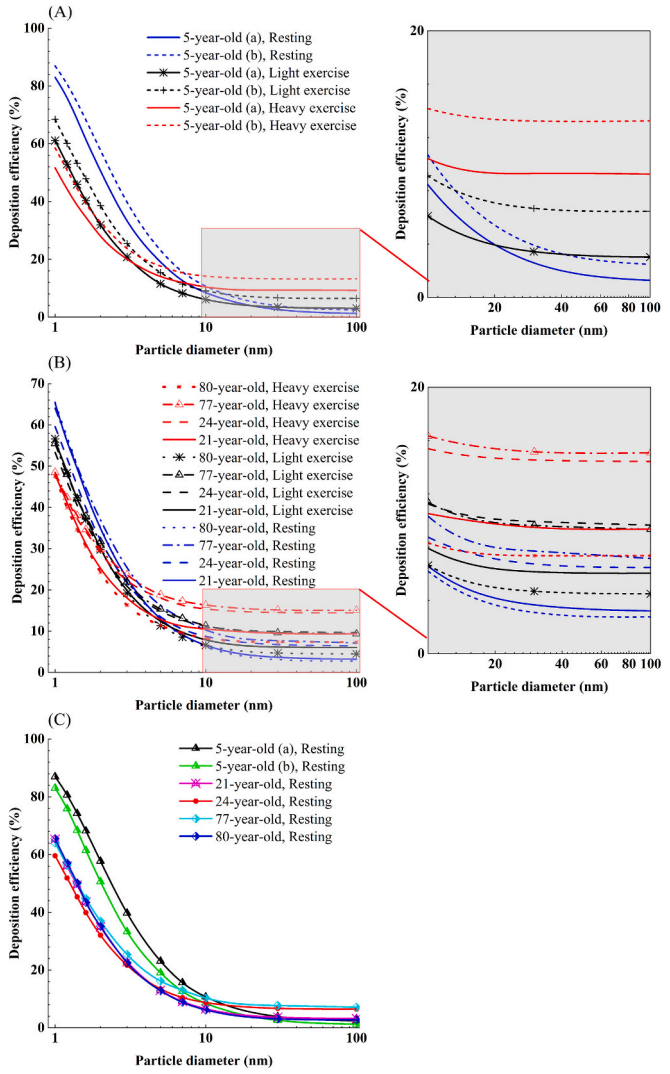

Fig. 11. Total deposition efficiency comparisons across varying inhalation flow rates corresponding to different activity levels: resting, light exercise, and heavy exercise - (A) child subjects; (B) adult and elderly subjects. Additionally, (C) presents a comparison of total deposition efficiency across age groups (children, adults, and the elderly) under a resting inhalation condition. Partial enlargement for A and B is to present more details for particles larger than 10 nm.

flow rates. In contrast, the 77-year-old and the 24-year-old subjects exhibited distinctive deposition efficiency curves. Slightly higher deposition levels (around 17.5 %) were evident in the 24-year-old and 77-year-old models for larger particle size under heavy exercise activity. This is attributed to the more promoted inertia impaction resulting from the greater curvature and narrower hydraulic diameter of their anterior nasal passages.

Following a thorough examination of deposition results respectively in child group and adult group, Fig. 11(C) provides a clear comparison between child and adult groups under the resting activity level. The selection of resting condition is deliberate, as it allows for the distinct revelation of inter-subject disparities, with Brownian-influenced particles benefiting from sufficient residence time under the lowest inhaled flow rate. In general, a substantial discrepancy was discernible between children and adults, while young adults and elder adults displayed similar results. It may highlight that the findings related to nanoparticle deposition based on adults may not be directly applicable to children. To illustrate, for the smallest particles at 1 nm, child models achieved an approximately 36 % higher deposition efficiency (ranging from 83 % to 87 %) compared to adult models (ranging from 60 % to 65 %). Compared to adult models, the immaturely narrow intranasal space in child subjects may promote the potential for highly diffusible particles to be captured by nasal surface. Additionally, it was observed that for larger particles (10 nm – 100 nm), around 2 % of particles were captured in child nasal cavities, a slightly lower proportion than in all selected adult models (approximately 6 %).

Fig. 12 compares deposition efficiency in subregions including vestibule, olfactory, main passage, and nasopharynx under light exercise flow rate conditions. Particles with diameter of 1 nm, 5 nm, and 100 nm were selected to represent the diffusion phenomenon varied from strongest to weakest.

In vestibule region, young adults exhibited stronger filtration performance than that of the elderly, which is more obvious for the 24-year-old subject. As discussed earlier, this subject has smaller hydraulic diameter in the vestibule and slightly higher complexity in the middle part of the vestibule. It led to non-uniform vortex flow in that area, enhancing the mix of particles and increase the possibility of particles colliding with the nasal surface. For child models, distinct inter-subject difference was observed for 1 nm, with deposition efficiency of 4.3 % for 5-year-old (a) and nearly doubled to 7.2 % for the other. It is not surprising since relatively pronounced vortices were observed in 5-year-old (b). Interestingly, in the phenomenon of low-level deposition efficiency for 100 nm particles, vestibule region of adult subjects seems to contribute considerable deposition. Compared to children, the mature nasal vestibule in adults is more effective at filtering particles before they enter the main passage. In the olfactory region, children exhibited apparently higher deposition efficiency for all particle size (value as high as around 5.5 % at 1 nm), while lower but varied results was found among adult groups. The data was consistent with proportionately more flow passing through the upper passage where olfactory located as seen in Fig. 7. Our previous study also provided quantitative evidence of fractional flow in olfactory region (Dong et al., 2021b). The main respiratory region, with largest area among four subregions, undertakes the primary filtering task since high level deposition efficiency was observed here, with values fluctuated between 36.3 % to 43.9 %. Consistent with the higher complexity of middle passage observed earlier in the elderly, their deposition efficiency in main passage was relatively higher than that of young adult. The nasopharynx, situated in the posterior of nasal airway, captured very few particles because of the limited number of untrapped particles entering that region.

3.5. Nasal deposition prediction with combined diffusion parameter

For the highly diffusional particles (< 200 nm) dominated by Brownian forces, extensive studies have developed several numerical models to predict the deposition efficiency. To achieve this, existing studies introduced different non-dimensional dynamics parameters to establish empirical models, and assessed its correlation with deposition efficiency. Cheng, et al. (Cheng et al., 1988) mentioned that the deposition data can be well fitted by a theoretical model based on a circular straight pipe which incorporated the inhalation flow rate Q and diffusion parameter coefficient D that considered was to be a fundamental parameter to express the diffusive process in precipitation kinetics (Eq. (10)). Then other studies paid efforts to analyse the dependence of deposition efficiency on the particle diffusion coefficient and the inhalation flow rate by utilizing different models (Cheng et al., 1995a; Xi et al., 2012; Cheng et al., 1995b). However, the deposition differences caused by the distinct age and apparent inter-subject variation of nasal airways has been shown to be important by previous studies, so that nasal geometrical dimensions, such as cross section area, mean perimeter, and total surface area, were used to try to correlate nasal deposition efficiency (Cheng et al., 1996a; Cheng et al., 1996b).

Notably, Schroeter, et al. (Schroeter et al., 2013) proposed a solution, that using the diffusion parameter Δ containing geometrical terms and Schmidt number S_C, to solving the impact of age-related geometry variation on deposition efficiency based on rhesus monkey nasal models.

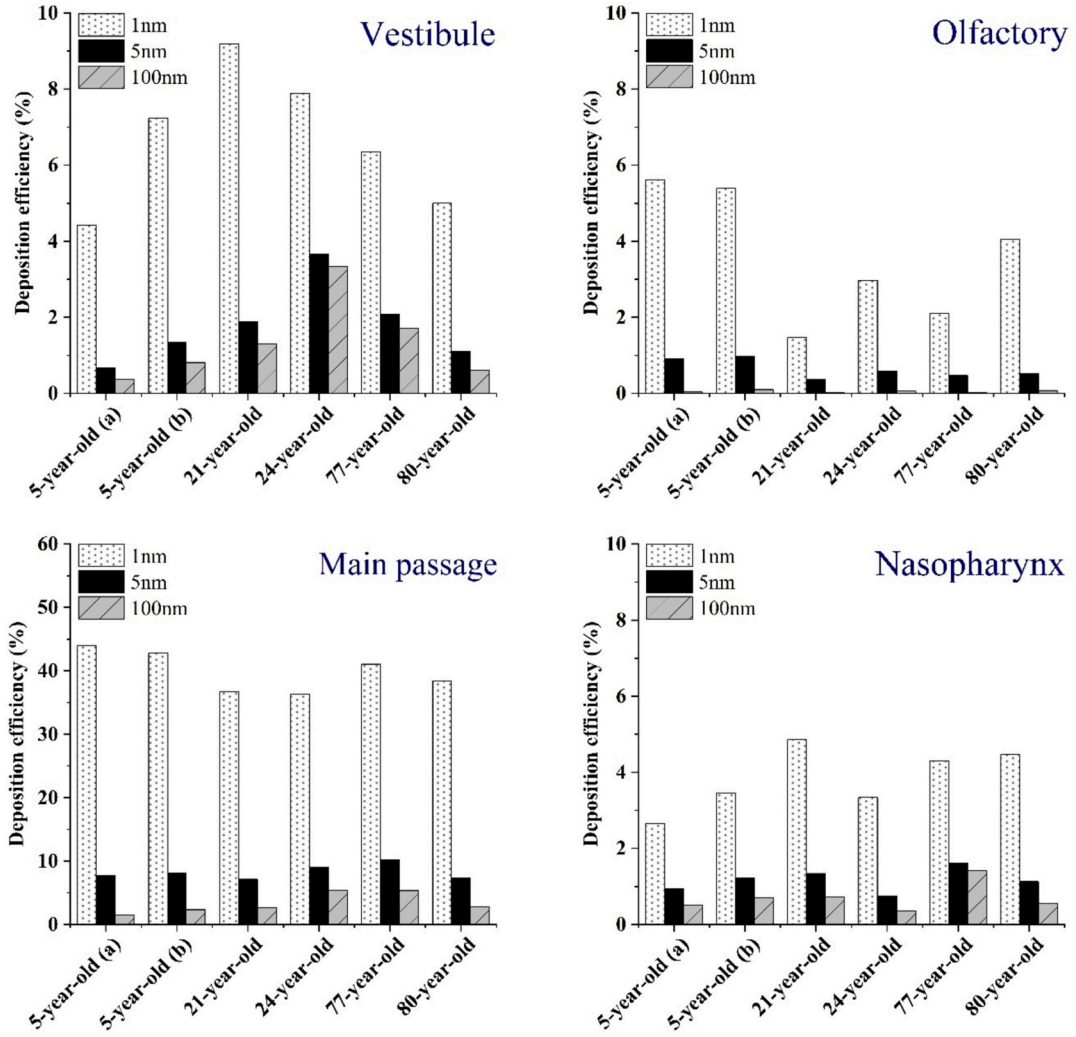

Fig. 12. Regional deposition efficiency at light exercise flow rates with selected particle diameter of 1 nm (high diffusion), 5 nm (weaker diffusion), and 10 nm (weakest diffusion). Subregions include vestibule, olfactory, main passage, and nasopharynx region.

Their effectiveness on representing deposition data on other monkey nasal models with inter-subject anatomical variation was later emphasized by Dong, et al. (Dong et al., 2021a). These quantified terms were earlier assessed in the study by Ingham (Ingham, 1991), which reported they can well predict the nanoparticle deposition efficiency for a circular pipe. Thus, the terms, that containing geometrical features as well as particle diffusivity and airflow rate, were considered to be reasonable to assess if the age-related impact on human nasal deposition can be quantified.

The diffusion parameter Δ is defined as:

$$\Delta = \frac{\widetilde{L}}{Pe} \bullet \widetilde{d_C} \tag{8}$$

where $\widetilde{L} = L/L_0$ is nondimensionalized characteristic length of nasal airway, L is characteristic length of nasal airway. L is measured by an arc curve from nostrils to the end of nasopharynx, which can be referred to Fig. 3 for more details. L_0 is standard measurement unit of 1 m. $\widetilde{d_C} = d_C/L_0$ is nondimensionalized inner characteristic diameter of nasal airway, d_C is inner characteristic diameter of nasal airway, $d_C = 2\sqrt{V/\pi L}$, where V is volume. Pe is Peclet number defined by:

$$Pe = d_C \bullet \frac{U}{D} \tag{9}$$

where U stands for characteristic airflow velocity across nasal airway, D denotes the molecular diffusivity of particles in the air,

$$D = \frac{k_B T C_C}{3\pi\mu d_P} \tag{10}$$

here k_B is Boltzmann's constant, T is absolute room temperature, C_C is Cunningham slip correction factor defined in the Method section, μ is viscosity of air (1.85×10^{-5} kg/m•s), and d_P is particle diameter.

It is noted that to develop an accurate correlation between deposition efficiency and parameters, characteristic airflow velocity U was calculated based on 17 cross-sectional slices along arc-length throughout nasal passage for each model.

Also, the Schmidt number S_C is represented by:

$$S_C = \frac{\nu}{D} \tag{11}$$

where ν is the kinematic viscosity of air at the room temperature (1.5×10^{-5} m^2/s).

Then a combined diffusion parameter, expressed as $Sc^a\Delta^b$, was employed as the x-axis to correlate the deposition efficiency. Coefficient a and b are constant power index to describe the dependence on the parameters, which is distinguish by fitted conditions for total and each subregion.

The prediction for total deposition efficiency can be well represented with the combined diffusion parameters as presented in Fig. 13. It

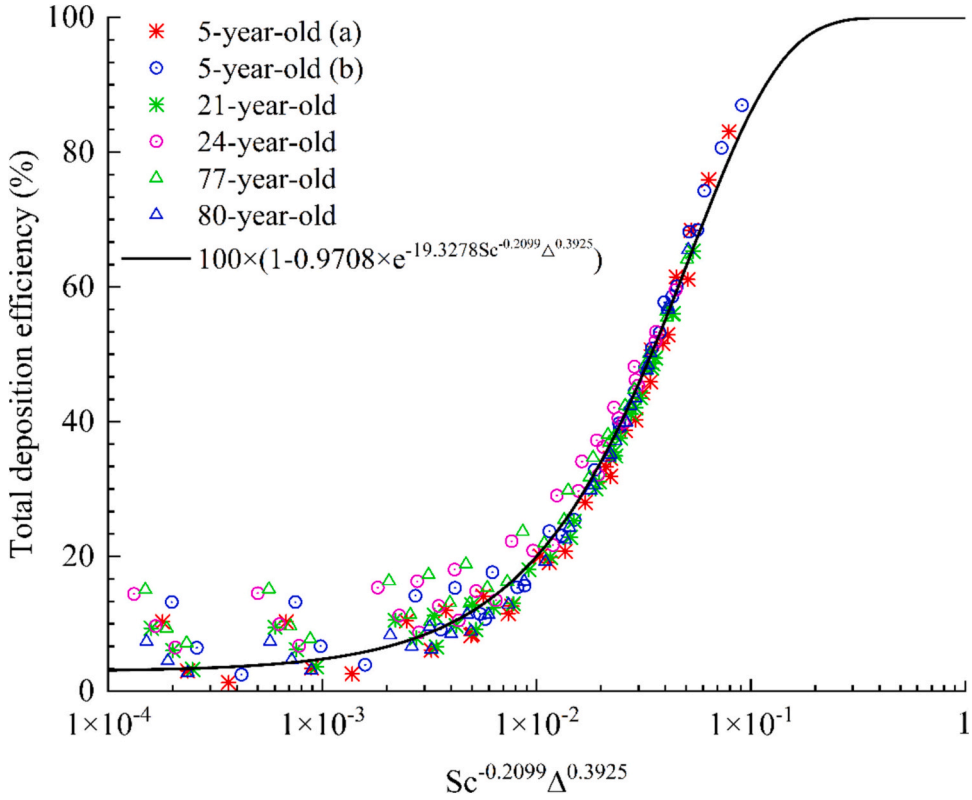

Fig. 13. Total deposition efficiency (%) as a function of the combined diffusion parameter: $Sc^{-0.2099}\Delta^{0.3925}$.

should be mentioned that dataset of each modal considered all inhalation flow rates for three activity levels, to provide convincing evidence if the correlation is universal for real life situations. This correlation fitted best when exponent coefficients were chosen as a = −0.2099 and b = 0.3925 with a R-squared value of 0.78. The correlation for the best fitting curve is:

$$DE_{total} = 100 \times \left(1 - 0.9708 \times e^{-19.3278 \times Sc^{-0.2099}\Delta^{0.3925}}\right)$$

Overall, the combined X-axis ranged between 1×10^{-4} to 0.1, where larger X-axis value represents smaller particle size. It can be seen that the deposition data trend to be noisier and less well represented by the fitted curve when the combined diffusion parameter is smaller than 0.01. This is the region where the deposition is less well represented by the theoretical model of Brownian diffusion as the deposition efficiency is at a low level for these lower values of the combined diffusion parameter. Moreover, larger combined diffusion parameter near 0.1 data points were all contributed by child models. It can be explained by the narrower characteristic diameter and moderate flow rate for children nasal airway, which contributed to larger diffusion parameter Δ. Although huge anatomical differences existed between age groups, results for each model appear to collapse into one curve. The results emphasized that the combined parameter had a good capability in bridging age-related anatomical differences due to distinct age, encouraging further exploration in important subregions.

Three subjects from the Validation Group—a 5-year-old female child, a 32-year-old female adult, and an 87-year-old elderly male—were used to further validate the robustness of the developed correlation. The same meshing method and numerical model were employed for simulations of these additional models. In Fig. 14, the particle deposition efficiencies for these three models were overlaid onto the total deposition efficiency curve originally developed from the six subjects in the Development Group. The deposition data showed strong alignment with the prediction curve, suggesting that the combined diffusion parameter can adequately accommodate age-related anatomical differences.

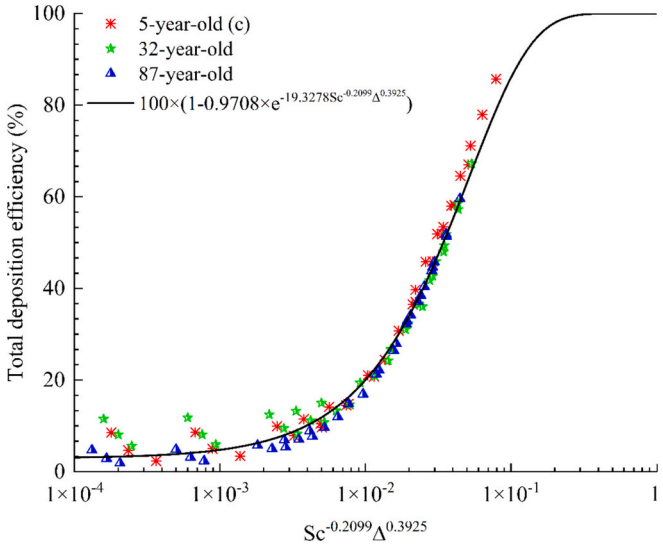

Fig. 14. Comparison of total deposition efficiency (%) of additional models from the Validation Group with the derived total deposition efficiency curve based on the original six models from the Development Group.

As discussed earlier, nasal epithelium, including squamous epithelium (vestibule), respiratory epithelium (main passage), and olfactory epithelium (olfactory), may experience airborne toxicant-induced epithelial lesions, which are generally dependent on site-specific dose and the sensitivity of epithelium to the chemicals. Thus, the correlations for total deposition efficiency are also applied to subregional prediction and modified for a site-specific prediction (Fig. 15). The most sufficient

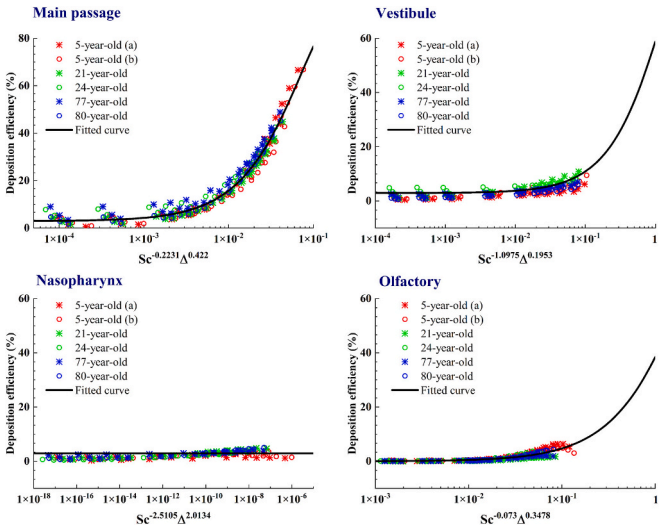

Fig. 15. Subregional deposition efficiency (%) of main passage, vestibule, nasopharynx, and olfactory region. Regional data and associated fitted curve were plotted respectively as a function of the combined diffusion parameters: $Sc^{-0.2311}\Delta^{0.422}$, $Sc^{-1.0975}\Delta^{0.1953}$, $Sc^{-2.5105}\Delta^{2.0134}$, and $Sc^{-0.073}\Delta^{0.3478}$.

exponents for the combined diffusion parameter in each region are: (I) Main respiratory region: $a = -0.2231$, $b = 0.422$ (II) Vestibule region: $a = -1.0975$, $b = 0.1953$ (III) Nasopharynx region: $a = -2.5105$, $b = 2.0134$ (IV) Olfactory region: $a = -0.073$, $b = 0.3478$.

Main respiratory region contributing the most of deposition efficiency in both children and adults, and the results almost collapse into each other both in children and adults. To achieve the best-fit performance, the exponent b increased to 0.422, which reflected a higher dependence on diffusion parameter, Δ, compared to that of the total deposition efficiency. As discussed earlier, the shape complexity of the main respiratory region exhibited a significant increase, promoting vortex and recirculation flow streams which contribute to particle deposition. In that situation, higher dependence on Δ that incorporates geometrical parameters may be reasonable. In contrast, the vestibule correlation exhibited weaker dependence on Δ but higher dependence on Sc. This suggests that Brownian motion of particles is the dominant phenomenon influencing vestibular filtration, rather than geometric factors. It should be noted that olfactory region was highly influenced by the airflow velocity and geometry due to the extremely large exponent b.

Similarly, the subregional deposition data of models from the Validation Group was compared with the prediction curves extracted earlier (Fig. 16). Overall, good agreement was achieved for the predictions in the main passage, vestibule, nasopharynx, and olfactory regions. Although the results for the 5-year-old (c) model showed minor deviations from the prediction curve, they remained within an acceptable range. This comparison supports that the combined diffusion parameters can effectively address age-related anatomical differences. However, as noted in the limitations of the current study, these correlations may need to be refined with a larger subject pool in future studies.

4. Conclusions

This study provides comprehensive analysis of the age-related anatomical differences in human nasal airways and their effects on airflow behaviour and ultrafine particle transport. By reconstructing nasal cavity models across various age groups – children, adults, and the elderly - we gained substantial insights into how anatomical variations affect inhalation toxicology.

1) Anatomical variations: The nasal cavities of children, with the cylindrical-like vestibules and narrower passages, facilitate a more uniform airflow, markedly differing from the complex airways of adults. Notably, the nasal anatomy becomes more intricate among the elderly, peaking in complexity in the middle of passages, which influences vortex formation and associated regional particle deposition.
2) Precise deposition analysis: Our findings highlight the inter-subject disparities in both overall and subregional deposition across age groups, particularly between children and adults. However, overall deposition profiles remain relatively similar. Further exploration in different functional subregions reveals that the adult nasal structure in the vestibule is more conducive to capturing particles. Additionally, olfactory deposition, exhibiting high sensitivity to local flow, is more pronounced in children than in adults.
3) Prediction and cross-age extrapolation: The intricate interplay between anatomical variations from childhood to adulthood and deposition efficiency is critical for predictions of nasal deposition. A novel approach is provided for predicting nasal ultrafine particle deposition efficiency across age groups, by introducing combined

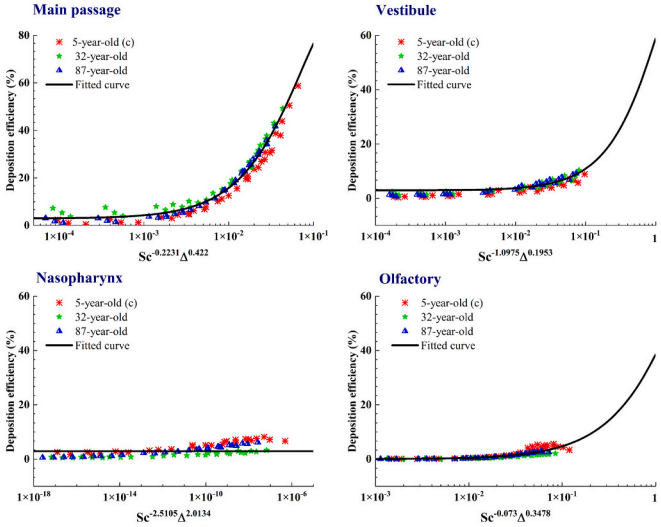

Fig. 16. Comparison of subregional deposition efficiency (%) of additional models from the Validation Group with the prediction curves for subregions, including the main passage, vestibule, nasopharynx, and olfactory regions.

diffusion parameters (expressed as $Sc^a\Delta^b$). To express age-related anatomical variations, geometrical terms, including volume, length, and inner diameter, are accounted for as characteristic dimensions for each nasal cavity. Incorporating correlations based on target regions, this approach performs reliably for prediction across subjects of different ages. It paves the way for future research in inhalation toxicology and respiratory drug delivery in populations of varied ages.

4.1. Limitations of current study

We acknowledge several limitations of current study. Firstly, potential variations in nasal dimensions due to physiological factors, such as nasal cycle or congestion, were not considered. Additionally, the influence of gender or ethnic differences was not considered at this stage of investigation. These might influence the BMI (based on height/weight ratio) or the respiratory parameters (*e.g.*, tidal volume), which are important for understanding human inhalation activity. Apparently, obtaining high-quality CT scans for CFD research studies in human volunteers presents significant challenges. Distributing subjects across categories such as age, sex, race, or health status (*e.g.*, healthy *vs.* diseased) is particularly difficult due to the high costs and the need for regulatory approvals to justify X-ray dose. Securing approval from funding agencies, especially for studies that require recruiting volunteers categorised by age and ensuring sufficient sample sizes in each group, adds further complexity. While we acknowledge these inherent limitations, building a comprehensive nasal subject model collection that encompasses diversity in age, sex, ethnicity, and health status falls outside the scope and capacity of the present project. Like most researchers in this field, we are limited to using existing data, which makes it impossible to include African American samples in this study. Additionally, the use of steady inhalation flow rates simplified the effects of realistic breathing waveforms and focused on time-averaged outcomes of particle deposition. Future studies will consider a larger and more diverse subject pool, as well as realistic unsteady inhalation flow conditions, to further improve the present research findings.

CRediT authorship contribution statement

Qinyuan Sun: Writing – original draft, Visualization, Validation, Formal analysis, Data curation, Conceptualization. **Ya Zhang:** Resources, Methodology, Conceptualization. **Lin Tian:** Writing – review & editing, Supervision, Conceptualization. **Jiyuan Tu:** Writing – review & editing, Supervision, Methodology, Conceptualization. **Richard Corley:** Writing – review & editing, Resources, Conceptualization. **Andrew P. Kuprat:** Writing – review & editing, Resources, Conceptualization. **Jingliang Dong:** Writing – review & editing, Visualization, Validation, Supervision, Project administration, Funding acquisition, Conceptualization.

Declaration of competing interest

The authors declare that they have no known competing financial interests or personal relationships that could have appeared to influence the work reported in this paper.

Acknowledgments

This study was funded by the Australian Research Council [Project ID: DE210101549].

Appendix

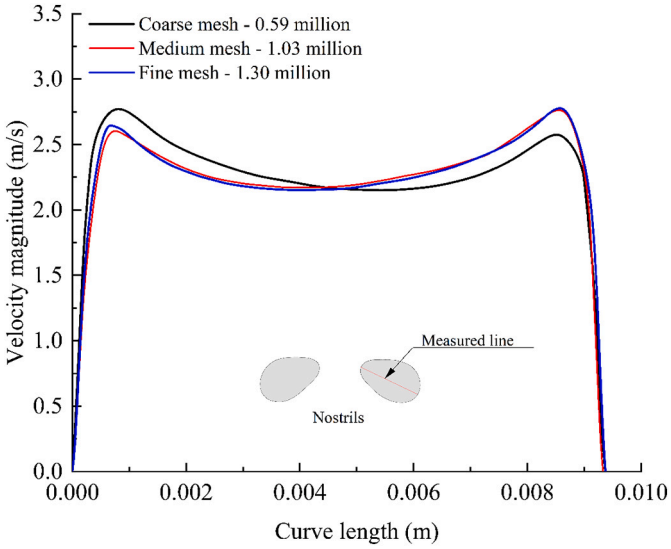

Fig. A1. The mesh independent test with three mesh configurations: coarse mesh with 0.57 million grids, medium mesh with 1.03 million grids, and fine mesh with 1.3 million grids.

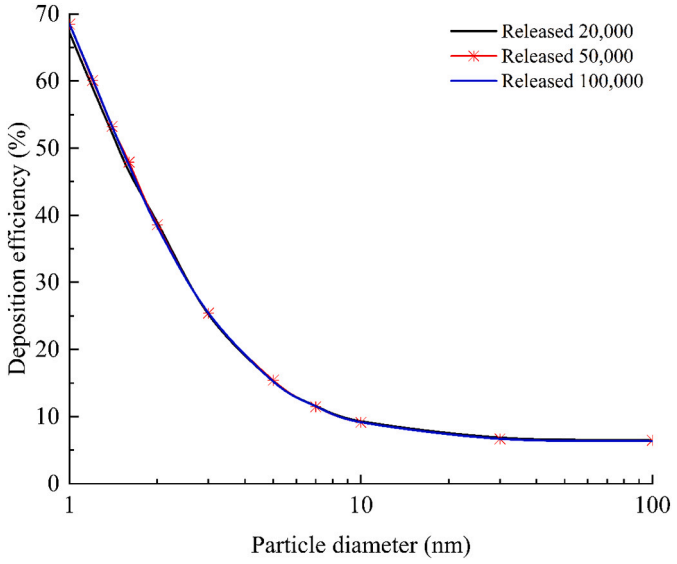

Fig. A2. Independent test of particle released number. 20,000, 50,000, 100,000 number of particles were respectively released uniformly at the hemisphere surface.

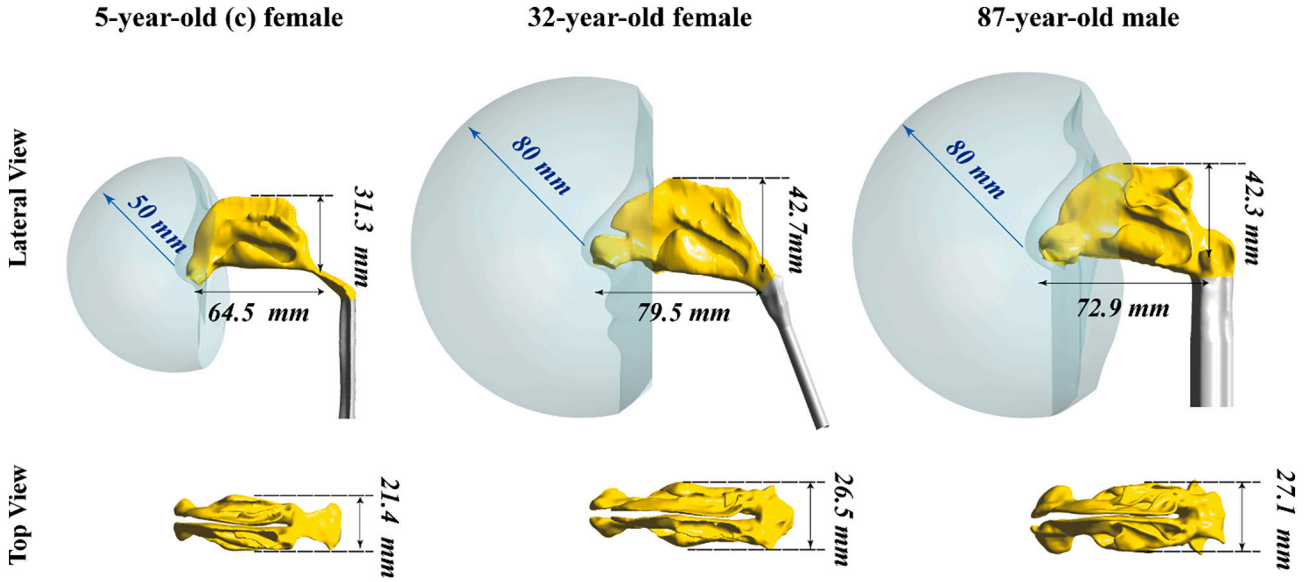

Fig. A3. Geometry of additional nasal models: a 5-year-old (c) female, a 32-year-old female, and an 87-year-old male. Height and length of each nasal cavity were marked in the lateral view and width were marked in the top view. A spherical breathing zone is attached to the exterior facial features of each nasal geometry, with a diameter of 50 mm for child subjects and 80 mm for adult subjects.

Table A1
Demographic information of additional subjects.

Label	Age (years)	Gender
5-year-old (c)	5	Female
32-year-old	32	Female
87-year-old	87	Male

Data availability

The data that support the findings of this study are available on request from the corresponding author. The data are not publicly available due to privacy or ethical restrictions.

References

Çakmak, Ö., Coşkun, M., Çelik, H., Büyüklü, F., Özlüoğlu, L.N., 2003. Value of acoustic Rhinometry for measuring nasal valve area. Laryngoscope 113 (2), 295–302. https://doi.org/10.1097/00005537-200302000-00018.

Cheng, K.H., Cheng, Y.S., Yeh, H.C., Swift, D.L., 1995b. Deposition of ultrafine aerosols in the head airways during natural breathing and during simulated breath holding using replicate human upper airway casts. Aerosol Sci. Technol. 23 (3), 465–474. https://doi.org/10.1080/02786829508965329.

Cheng, K.-H., Cheng, Y.-S., Yeh, H.-C., Guilmette, R.A., Simpson, S.Q., Yang, Y.-H., Swift, D.L., 1996a. In vivo measurements of nasal airway dimensions and ultrafine aerosol deposition in the human nasal and oral airways. J. Aerosol Sci. 27 (5), 785–801. https://doi.org/10.1016/0021-8502(96)00029-8.

Cheng, Y.S., Yeh, H.C., Guilmette, R.A., Simpson, S.Q., Cheng, K.H., Swift, D.L., 1996b. Nasal deposition of ultrafine particles in human volunteers and its relationship to airway geometry. Aerosol Sci. Technol. 25 (3), 274–291. https://doi.org/10.1080/02786829608965396.

Cheng, Y.-S., Yamada, Y., Yeh, H.-C., Swift, D.L., 1988. Diffusional deposition of ultrafine aerosols in a human nasal cast. J. Aerosol Sci. 19 (6), 741–751. https://doi.org/10.1016/0021-8502(88)90009-2.

Cheng, Y.-S., Smith, S.M., Yeh, H.-C., Kim, D.-B., Cheng, K.-H., Swift, D.L., 1995a. Deposition of ultrafine aerosols and Thoron progeny in replicas of nasal Airways of Young Children. Aerosol Sci. Technol. 23 (4), 541–552. https://doi.org/10.1080/02786829508965336.

Cochran, C.S., Ducic, Y., DeFatta, R.J., 2007. Restorative rhinoplasty in the aging patient. Laryngoscope 117 (5), 803–807. https://doi.org/10.1097/01.mlg.0000248240.72296.b9.

Cole, P., Roithmann, R., 1996. The nasal valve and current technology. Am. J. Rhinol. 10 (1), 23–38. https://doi.org/10.2500/105065896781795111.

Darquenne, C., 2020. Deposition mechanisms. J. Aerosol Med. Pulm. Drug Deliv. 33 (4), 181–185. https://doi.org/10.1089/jamp.2020.29029.cd.

Dong, J., Ma, J., Shang, Y., Inthavong, K., Qiu, D., Tu, J., Frank-Ito, D., 2018. Detailed nanoparticle exposure analysis among human nasal cavities with distinct vestibule phenotypes. J. Aerosol Sci. 121, 54–65. https://doi.org/10.1016/j.jaerosci.2018.05.001.

Dong, J., Ma, J., Tian, L., Inthavong, K., Ito, K., Tu, J., 2021a. Numerical analysis of nanoparticle transport and deposition in a cynomolgus monkey nasal passage. Int. J. Numer. Methods Biomed. Eng. 37 (2), e3414. https://doi.org/10.1002/cnm.3414.

Dong, J., Sun, Q., Shang, Y., Zhang, Y., Tian, L., Tu, J., 2021b. Numerical comparison of inspiratory airflow patterns in human nasal cavities with distinct age differences. Int. J. Numer. Methods Biomed. Eng. https://doi.org/10.1002/cnm.3565.

Edelstein, D.R., 1996. Aging of the Normal nose in adults. Laryngoscope 106 (S81), 1–25. https://doi.org/10.1097/00005537-199609001-00001.

Elad, D., Wolf, M., Keck, T., 2008. Air-conditioning in the human nasal cavity. Respir. Physiol. Neurobiol. 163 (1), 121–127. https://doi.org/10.1016/j.resp.2008.05.002.

Garcia, G.J.M., Schroeter, J.D., Kimbell, J.S., 2015. Olfactory deposition of inhaled nanoparticles in humans. Inhal. Toxicol. 27 (8), 394–403. https://doi.org/10.3109/08958378.2015.1066904.

Golshahi, L., Finlay, W.H., Olfert, J.S., Thompson, R.B., Noga, M.L., 2010. Deposition of inhaled ultrafine aerosols in replicas of nasal Airways of Infants. Aerosol Sci. Technol. 44 (9), 741–752. https://doi.org/10.1080/02786826.2010.488256.

Harkema, J.R., Carey, S.A., Wagner, J.G., 2006. The nose revisited: a brief review of the comparative structure, function, and Toxicologic pathology of the nasal epithelium. Toxicol. Pathol. 34 (3), 252–269. https://doi.org/10.1080/01926230600713475.

Huang, Z.L., Wang, D.Y., Zhang, P.C., Dong, F., Yeoh, K.H., 2001. Evaluation of nasal cavity by acoustic rhinometry in Chinese, Malay and Indian ethnic groups. Acta Otolaryngol. 121 (7), 844–848. https://doi.org/10.1080/00016480152602311.

ICRP, 1994. Human Respiratory Tract Model for Radiological Protection. *ICRP*, p. 488. Publication 66 (Ann. ICRP 24 (1–3)).

Ingham, D.B., 1991. Diffusion of aerosols in the entrance region of a smooth cylindrical pipe. J. Aerosol Sci. 22 (3), 253–257. https://doi.org/10.1016/S0021-8502(05)80003-5.

Inthavong, K., Tu, J., Ahmadi, G., 2009. Computational modelling of gas-particle flows with different particle morphology in the human nasal cavity. J. Comput. Multiphase Flows 1 (1), 57–82. https://doi.org/10.1260/175748209787387061.

Inthavong, K., Zhang, K., Tu, J., 2011. Numerical modelling of nanoparticle deposition in the nasal cavity and the tracheobronchial airway. Comput. Methods Biomech. Biomed. Engin. 14 (7), 633–643. https://doi.org/10.1080/10255842.2010.493510.

Kalmovich, L.M., Elad, D., Zaretsky, U., Adunsky, A., Chetrit, A., Sadetzki, S., Segal, S., Wolf, M., 2005. Endonasal geometry changes in elderly people: acoustic Rhinometry measurements. J. Gerontol. A 60 (3), 396–398. https://doi.org/10.1093/gerona/60.3.396.

Khezri, K., Saeedi, M., Maleki Dizaj, S., 2018. Application of nanoparticles in percutaneous delivery of active ingredients in cosmetic preparations. Biomed. Pharmacother. 106, 1499–1505. https://doi.org/10.1016/j.biopha.2018.07.084.

Kim, S.W., Mo, J.H., Kim, J.W., Kim, D.Y., Rhee, C.S., Lee, C.H., Min, Y.G., 2007. Change of nasal function with aging in Korean. Acta Otolaryngol. 127 (Suppl. 558), 90–94. https://doi.org/10.1080/03655230701624939.

Loftus, P.A., Wise, S.K., Nieto, D., Panella, N., Aiken, A., DelGaudio, J.M., 2016. Intranasal volume increases with age: computed tomography volumetric analysis in adults. Laryngoscope 126 (10), 2212–2215. https://doi.org/10.1002/lary.26064.

Moghadas, H., Abouali, O., Faramarzi, A., Ahmadi, G., 2011. Numerical investigation of septal deviation effect on deposition of nano/microparticles in human nasal passage. Respir. Physiol. Neurobiol. 177 (1), 9–18. https://doi.org/10.1016/j.resp.2011.02.011.

Munkholm, M., Mortensen, J., 2014. Mucociliary clearance: pathophysiological aspects. Clin. Physiol. Funct. Imaging 34 (3), 171–177. https://doi.org/10.1111/cpf.12085.

Noback, M.L., Harvati, K., Spoor, F., 2011. Climate-related variation of the human nasal cavity. Am. J. Phys. Anthropol. 145 (4), 599–614. https://doi.org/10.1002/ajpa.21523.

Parkes, M.L., Kamer, F.M., 1973. The mature nose. Laryngoscope 83 (2), 157–166. https://doi.org/10.1288/00005537-197302000-00001.

Proença de Oliveira-Maul, J., Barbosa de Carvalho, H., Goto, D.M., Maia, R.M., Fló, C., Barnabé, V., Franco, D.R., Benabou, S., Perracini, M.R., Jacob-Filho, W., Saldiva, P. H.N., Lorenzi-Filho, G., Rubin, B.K., Nakagawa, N.K., 2013. Aging, diabetes, and hypertension are associated with decreased nasal Mucociliary clearance. Chest 143 (4), 1091–1097. https://doi.org/10.1378/chest.12-1183.

Rahman, A., Sarkar, A., Yadav, O.P., Achari, G., Slobodnik, J., 2021. Potential human health risks due to environmental exposure to nano- and microplastics and knowledge gaps: a scoping review. Sci. Total Environ. 757, 143872. https://doi.org/10.1016/j.scitotenv.2020.143872.

Rahman, M.M., Vuorinen, V., Taghinia, J., Larmi, M., 2019. Wall-distance-free formulation for SST k-ω model. Eur. J. Mech. B/Fluids 75, 71–82. https://doi.org/10.1016/j.euromechflu.2018.11.010.

Sakakura, Y., Ukai, K., Majima, Y., Murai, S., Harada, T., Miyoshi, Y., 1983. Nasal Mucociliary clearance under various conditions. Acta Otolaryngol. 96 (1–2), 167–173. https://doi.org/10.3109/00016488309132888.

Samoliński, B.K., Grzanka, A., Gotlib, T., 2007. Changes in nasal cavity dimensions in children and adults by gender and age. Laryngoscope 117 (8), 1429–1433. https://doi.org/10.1097/MLG.0b013e318064e837.

Schroeter, J.D., Kimbell, J.S., Asgharian, B., Tewksbury, E.W., Singal, M., 2012. Computational fluid dynamics simulations of submicrometer and micrometer particle deposition in the nasal passages of a Sprague-Dawley rat. J. Aerosol Sci. 43 (1), 31–44. https://doi.org/10.1016/j.jaerosci.2011.08.008.

Schroeter, J.D., Asgharian, B., Price, O.T., McClellan, G.E., 2013. Computational fluid dynamics simulations of inhaled nano- and microparticle deposition in the rhesus monkey nasal passages. Inhal. Toxicol. 25 (12), 691–701. https://doi.org/10.3109/08958378.2013.835889.

Seaton, A., Godden, D., MacNee, W., Donaldson, K., 1995. Particulate air pollution and acute health effects. Lancet 345 (8943), 176–178. https://doi.org/10.1016/S0140-6736(95)90173-6.

Seaton, A., Tran, L., Aitken, R., Donaldson, K., 2010. Nanoparticles, human health hazard and regulation. J. R. Soc. Interface 7 (suppl_1), S119–S129. https://doi.org/10.1098/rsif.2009.0252.focus.

Sforza, C., Grandi, G., De Menezes, M., Tartaglia, G.M., Ferrario, V.F., 2011. Age- and sex-related changes in the normal human external nose. Forensic Sci. Int. 204 (1), 205.e1–205.e9. https://doi.org/10.1016/j.forsciint.2010.07.027.

Shang, Y., Dong, J., Inthavong, K., Tu, J., 2015b. Comparative numerical modeling of inhaled micron-sized particle deposition in human and rat nasal cavities. Inhal. Toxicol. 27 (13), 694–705. https://doi.org/10.3109/08958378.2015.1088600.

Shang, Y., Dong, J., He, F., Inthavong, K., Tian, L., Tu, J., 2022. Detailed comparative analysis of environmental microparticle deposition characteristics between human and monkey nasal cavities using a surface mapping technique. Sci. Total Environ. 853, 158770. https://doi.org/10.1016/j.scitotenv.2022.158770.

Shang, Y.D., Inthavong, K., Tu, J.Y., 2015a. Detailed micro-particle deposition patterns in the human nasal cavity influenced by the breathing zone. Comput. Fluids 114, 141–150. https://doi.org/10.1016/j.compfluid.2015.02.020.

Shi, H., Kleinstreuer, C., Zhang, Z., 2008. Dilute suspension flow with nanoparticle deposition in a representative nasal airway model. Phys. Fluids *20* (1). https://doi.org/10.1063/1.2833468.

Sun, Q., Dong, J., Zhang, Y., Tian, L., Tu, J., 2023. Numerical modelling of micron particle inhalation in a realistic nasal airway with pediatric adenoid hypertrophy: a virtual comparison between pre- and postoperative models. Front. Pediatr. 11. https://doi.org/10.3389/fped.2023.1083699.

Swift, D.L., Montassier, N., Hopke, P.K., Karpen-Hayes, K., Cheng, Y.-S., Yin Fong, S., Hsu Chi, Y., Strong, J.C., 1992. Inspiratory deposition of ultrafine particles in human nasal replicate cast. J. Aerosol Sci. 23 (1), 65–72. https://doi.org/10.1016/0021-8502(92)90318-P.

van der Heijden, P., Korsten-Meijer, A.G., van der Laan, B.F., Wit, H.P., Goorhuis-Brouwer, S.M., 2008. Nasal growth and maturation age in adolescents. Arch. Otolaryngol. Head Neck Surg. 134 (12), 1288–1293. https://doi.org/10.1001/archoto.2008.501.

Vaquero, C., Gutierrez-Cañas, C., Galarza, N., López de Ipiña, J.L., 2016. Exposure assessment to engineered nanoparticles handled in industrial workplaces: the case of alloying nano-TiO2 in new steel formulations. J. Aerosol Sci. 102, 1–15. https://doi.org/10.1016/j.jaerosci.2016.08.011.

Wang, W., Cao, Y., Okaze, T., 2021. Comparison of hexahedral, tetrahedral and polyhedral cells for reproducing the wind field around an isolated building by LES. Build. Environ. 195, 107717. https://doi.org/10.1016/j.buildenv.2021.107717.

Wen, J., Inthavong, K., Tu, J., Wang, S., 2008. Numerical simulations for detailed airflow dynamics in a human nasal cavity. Respir. Physiol. Neurobiol. 161 (2), 125–135. https://doi.org/10.1016/j.resp.2008.01.012.

Xi, J., Berlinski, A., Zhou, Y., Greenberg, B., Ou, X., 2012. Breathing resistance and ultrafine particle deposition in nasal-laryngeal airways of a newborn, an infant, a child, and an adult. Ann. Biomed. Eng. 40 (12), 2579–2595. https://doi.org/10.1007/s10439-012-0603-7.

Yang, F., Wang, Y., Ma, R., Hu, Z., Zhao, J., Sun, S., Ren, H., Chen, X., Chen, J., Zheng, G., Ren, X., Tong, Z., Dong, J., Zhang, Y., 2024. Numerical investigation of corticosteroid aerosol transport characteristics for pediatric acute epiglottitis at different severity levels. Powder Technol. 433, 119175. https://doi.org/10.1016/j.powtec.2023.119175.

Yu, H., Thé, J., 2016. Validation and optimization of SST k-ω turbulence model for pollutant dispersion within a building array. Atmos. Environ. 145, 225–238. https://doi.org/10.1016/j.atmosenv.2016.09.043.

Zamankhan, P., Ahmadi, G., Wang, Z., Hopke, P.K., Cheng, Y.-S., Su, W.C., Leonard, D., 2006. Airflow and deposition of Nano-particles in a human nasal cavity. Aerosol Sci. Technol. 40 (6), 463–476. https://doi.org/10.1080/02786820600660903.

Zankl, A., Eberle, L., Molinari, L., Schinzel, A., 2002. Growth charts for nose length, nasal protrusion, and philtrum length from birth to 97 years. Am. J. Med. Genet. 111 (4), 388–391. https://doi.org/10.1002/ajmg.10472.